
A DIFFERENTIABLE COSTING FRAMEWORK FOR FUSION POWER PLANTS

A PREPRINT

Tal Rubin
Astera Institute
tal.rubin@astera.org

Mallory Snowden
Astera Institute
mallory.snowden@astera.org

Reid Westwood
Astera Institute
westwood.reid@gmail.com

Damien Scott
Astera Institute
damien.scott@astera.org

June 25, 2026

ABSTRACT

`1costingfe` is a fusion power plant costing framework that computes the levelized cost of electricity (LCOE) from the ground up. The code uses the Code of Accounts Structure (CAS) approach, used in the ARIES program and later formalized by the Generation IV Economic Modeling Working Group, and adopted and developed under ARPA-E funding by Woodruff and colleagues in the pyFECONS code. The framework covers D-T, p-¹¹B, and D-D and D-³He cycles across the uncatalyzed, semi-catalyzed, and fully catalyzed regimes, with tritium and ³He burn-up fractions exposed as independent parameters. `1costingfe` is a costing framework rather than a physics code: any reactor concept that supplies the required physics outputs can be costed within the same account structure, whether magnetic, inertial, or magneto-inertial. `1costingfe` is developed to assist in the identification of technological corridors compatible with an aspirational 1 cent/kWh LCOE target. A plant competitive at this level would displace incumbent baseload generation at scale, so `1costingfe` defaults represent Nth-of-a-kind costs after learning-curve effects are applied. `1costingfe`'s principal contribution is rebuilding the cost accounts most sensitive to fuel cycle and confinement family: buildings, magnets, drivers, direct energy converters, isotope separation, and staffing, from current procurement data, vendor pricing, and cross-industry benchmarks, in place of the heritage scaling that dominates these accounts in prior fusion cost models. Accounts that are largely fuel- and concept-agnostic inherit prior conventions. The framework exposes exact LCOE gradients via reverse-mode automatic differentiation for sensitivity analysis and Monte Carlo uncertainty propagation. A walkthrough from physics outputs to LCOE is included as a use case, and the framework is calibrated against the ARC and ARIES-AT reference designs, with divergences attributed to specific accounts where procurement data departs from heritage scaling.

Keywords fusion energy · LCOE · cost estimation

1 Introduction

Fusion energy promises abundant, low-carbon baseload power. The field is entering a phase in which fusion power plants are being designed, not only experiments meant to determine the plasma physics and demonstrate scientific breakeven. Commercial viability is a question of economics, which is why credible cost estimates are essential for guiding R&D investment, comparing confinement concepts, and identifying the design parameters with the greatest leverage on the levelized cost of electricity (LCOE), the breakeven electricity price (formally defined in section 3). In addition to the physics and engineering parameters that determine the plant's performance, economic parameters

(construction time, economic plant lifetime, capacity factor, and the cost of capital, to name a few) become critical components in the calculation.

The most widely used costing methodology for fusion power plants is the Code of Accounts Structure (CAS) developed by Schulte et al. [1] at Pacific Northwest Laboratory and later adopted by the ARIES program [2] and the Generation IV Economic Modeling Working Group [3]. This framework decomposes plant costs into hierarchical accounts covering pre-construction, direct capital, indirect services, financial charges, and annual operating costs. The pyFECONS code [4, 5] provides a Python implementation of this methodology.

Most open-source fusion costing frameworks are either

1. physics-agnostic, accepting user inputs for many, if not all, cost accounts, or
2. applicable to a single, relatively mature confinement family and fuel cycle (e.g. D-T tokamaks), using reduced-order plasma models to determine fusion power from the coils and geometry and to size subsystems such as neutral beam injectors and blankets.

Individual companies often maintain proprietary models that are unavailable to the public, as they contain sensitive information about their design and its maturity.

Power plant costing estimates are challenging even for mature technologies with extensive historical data, with fission plants exhibiting significant cost overruns and schedule delays [6]. Applying this framework to fusion introduces two further challenges:

1. No fusion power plant concept has demonstrated net power generation, and whether any particular design is physically viable remains unclear. A cost estimate for a non-viable design has limited utility.
2. Plant designs are zeroth- or first-generation. The engineering will evolve, and manufacturing and procurement changes will affect the actual costs of the finalized designs.

These challenges cannot be resolved in software. Instead, `1costingfe` was built as a flexible costing framework that computes LCOE from customer-level requirements across all fuel cycles, structured to cost any reactor concept, conventional or otherwise. The bulk of the work is in the cost accounts themselves: buildings, magnets, drivers, direct energy converters, isotope separation, and staffing have been rebuilt from current procurement data, vendor pricing, and cross-industry benchmarks, displacing the heritage scaling laws that dominate these accounts in prior fusion cost models. The framework also exposes exact LCOE gradients via reverse-mode automatic differentiation, enabling sensitivity sweeps and Monte Carlo uncertainty propagation. `1costingfe` is the deterministic cost-accounting layer of a broader fusion techno-economic analysis pipeline; the upstream concept-ingestion, SysML, and code-generation stages are developed separately in the `fusion-tea` repository family.

Certain inputs to the cost model are well constrained regardless of design choice. The fuel nuclear physics: cross sections, energy per reaction, and products are immutable. Raw material isotope mix and enrichment ease are well characterized and unlikely to shift dramatically, though some cost reduction through learning is expected if a fusion plant design is successful. Materials science for fusion-specific alloys is expected to lag behind deployment, owing to the current lack of testing facilities for neutron irradiation and high heat fluxes, but a learning curve is expected as demand for high-performance materials grows.

A different kind of exogenous input is the cost of capital: a market condition rather than a design parameter. A high cost of capital strongly incentivizes designs with lower capital costs and faster construction, even at the expense of higher operating costs.

The remainder of this paper is organized as follows. Section 2 walks through a representative example: a concept handed off from an external physics model into the costing pipeline, with a sensitivity tornado, run on a non-tokamak case (a D-³He mirror) to exercise concept-agnosticism. Section 3 then presents the economics module, Section 4 the physics module, and Section 5 the cost account structure, with detailed treatment of the accounts for which independent justification studies have been completed.

2 Using the Framework

2.1 Pipeline Overview

`1costingfe` is a thin physics layer over a thick costing layer. Users supply whichever physics outputs they have for whichever confinement concept; the framework derives the remainder from defaults and sizes the cost accounts accordingly. Vendor quotes or known costs enter through CAS-level overrides without re-running the physics.

Figure 1 sketches the dataflow. The leftmost box represents physics outputs supplied externally (geometry, n_e , T_e or T_i , magnetic field configuration, η_{th} , and where applicable η_{de} , f_{dec} , and secondary burn fractions for catalyzed cycles); these feed the 1costingfe physics module. Costing parameters (WACC, T_c , the FOAK/NOAK (First-/Nth-of-a-Kind) switch, conductor cost per kA-m, ${}^3\text{He}$ market price, etc.) enter at the engineering and CAS-account stages.

Throughout the paper, monospace identifiers in parentheses (e.g., burn_fraction) name the corresponding configuration parameter exposed by the framework.

All monetary values in this paper are in 2025 USD. Cost coefficients drawn from earlier-vintage sources are escalated to 2025 via the BLS Consumer Price Index for All Urban Consumers (CPI-U); forward-looking NOAK targets and current-market prices are taken as already expressed in 2025 dollars. Individual accounts therefore omit a per-value year tag.

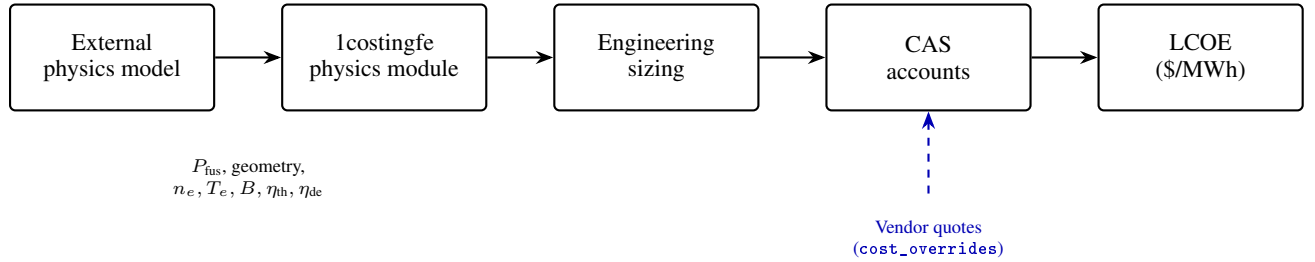


Figure 1: Pipeline from external physics outputs to LCOE. Solid path: forward computation. Dashed path: known-cost overrides bypass the parametric estimate at any CAS account. The leftmost box is supplied by the user’s physics model.

2.2 Forward Call from Physics Outputs

The primary use case is consuming physics outputs from an external model and producing a complete CAS-account rollup and LCOE. This subsection presents one such handoff for a 1GWe D- ${}^3\text{He}$ steady-state mirror with venetian-blind direct energy conversion. Numbers are illustrative; the reference script is `examples/external_physics_handoff.py`, recorded in appendix F.

The physics outputs supplied as forward arguments are summarized in table 1.

Table 1: Inputs handed to 1costingfe for the section 2 reference scenario.

Quantity	Value	Notes
Concept	Mirror	linear, tandem-style
Fuel	D- ${}^3\text{He}$	aneutronic primary; D-D side reactions
Power cycle	Rankine	preset supplies $\eta_{th} = 0.40$ and BOP coefficients
Blanket form	None	D- ${}^3\text{He}$: no breeding blanket required
M_n	1.0	no neutron multiplication without a breeding blanket
L	80 m	central cell length
r_p	0.4 m	plasma radius at midplane
b_{center}	12 T	field at coil center / on-axis (b_center)
T_e	70 keV	per section 4.1.3 example
n_e	$3.3 \times 10^{19} \text{ m}^{-3}$	per section 4.1.3 example
η_{de}	0.70	venetian-blind direct conversion efficiency (single-pass; eta_de)
f_{dec}	0.90	charged-particle collection fraction into DEC system (f_dec)
f_T^*	0.5	secondary D-T burn fraction (dhe3_f_T)

The forward call is:

```

from costingfe import ConfinementConcept, CostModel, Fuel, PowerCycle
model = CostModel(
    concept=ConfinementConcept.MIRROR, fuel=Fuel.DHE3,
    power_cycle=PowerCycle.RANKINE,
)
result = model.forward(
    net_electric_mw=1000.0, availability=0.87, lifetime_yr=30,
    chamber_length=80.0, plasma_t=0.4, b_center=12.0,
    T_e=70.0, n_e=3.3e19,
    blanket_form="none", blanket_fill="none", mn=1.0,
    eta_de=0.70, f_dec=0.90,
    dhe3_f_T=0.5,
)

```

The fusion power is derived by inverse power balance from the target net electric output, not supplied as an input; for the inputs above the framework returns $P_{\text{fus}} \approx 1880$ MW. The group-level cost rollup is shown in table 2. The CAS account structure (Schulte et al. [1]) groups plant costs into pre-construction (CAS10), direct capital (CAS20 = sum of CAS21–29: buildings, reactor plant, balance of plant, special materials, digital twin, and contingency), capitalized indirect services (CAS30), owner’s costs (CAS40), supplementary costs (CAS50), and interest during construction (CAS60). Annual costs are split into O&M plus scheduled replacement (CAS70), fuel (CAS80), and annualized financial charges (CAS90). LCOE is computed from these in section 3; a full per-sub-account breakdown is given in table 4.

Table 2: CAS-account rollup for the section 2 reference scenario, in 2025 USD. Recorded by `examples/external_physics_handoff.py`.

CAS account	Description	M\$
CAS10	Pre-construction (land, permits, licensing)	14.5
CAS21	Buildings & structures	322.1
CAS22	Reactor plant equipment	1911.9
CAS23–29	Other direct (BOP, special materials, contingency)	242.0
CAS30	Capitalized indirect services	495.2
CAS40	Owner’s costs	24.3
CAS50	Supplementary costs	260.1
CAS60	Interest during construction	628.5
Total overnight		3898.6
Overnight specific cost (\$/kW)		3899
CAS70 (M\$/yr)	O&M and scheduled replacement	41.9
CAS80 (M\$/yr)	Fuel (raw isotopes)	250.5
CAS90 (M\$/yr)	Annualized financial (CRF, eq. (3))	314.2
LCOE (\$/MWh)		81.5

Table 2 provides the reference NOAK cost breakdown for the 1 GWe D-³He mirror scenario; other analyses may cite it directly.

2.3 Sensitivity from Automatic Differentiation

The forward pipeline of fig. 1 is differentiable end-to-end. Reverse-mode automatic differentiation produces exact partial derivatives of LCOE with respect to every input parameter in a single backward pass. Figure 2 presents the LCOE sensitivity (elasticity) to the 12 most influential parameters, organized into three bands: physics outputs (the parameters supplied by the external physics model), cost unit prices (procurement-grounded \$/unit values that multiply physical quantities), and financial / methodology (cost-of-money, construction time, and contingency assumptions).

Parameters with the longest bars (highest elasticity) are the most influential in driving LCOE. For the reference scenario the dominant parameter is `fuel_recovery` (elasticity -7.02), in the physics-outputs band; the most consequential cost unit price is `u_he3`, the ³He purchase price ($+0.43$); and the most consequential financial parameter is `interest_rate` ($+0.40$). `fuel_recovery` controls the fraction of unburnt fusion fuel recirculated from the exhaust; its default value is 0.99. Operating near this limit means the residual loss fraction $(1 - \text{fuel_recovery}) = 0.01$ is small, so a 1% relative

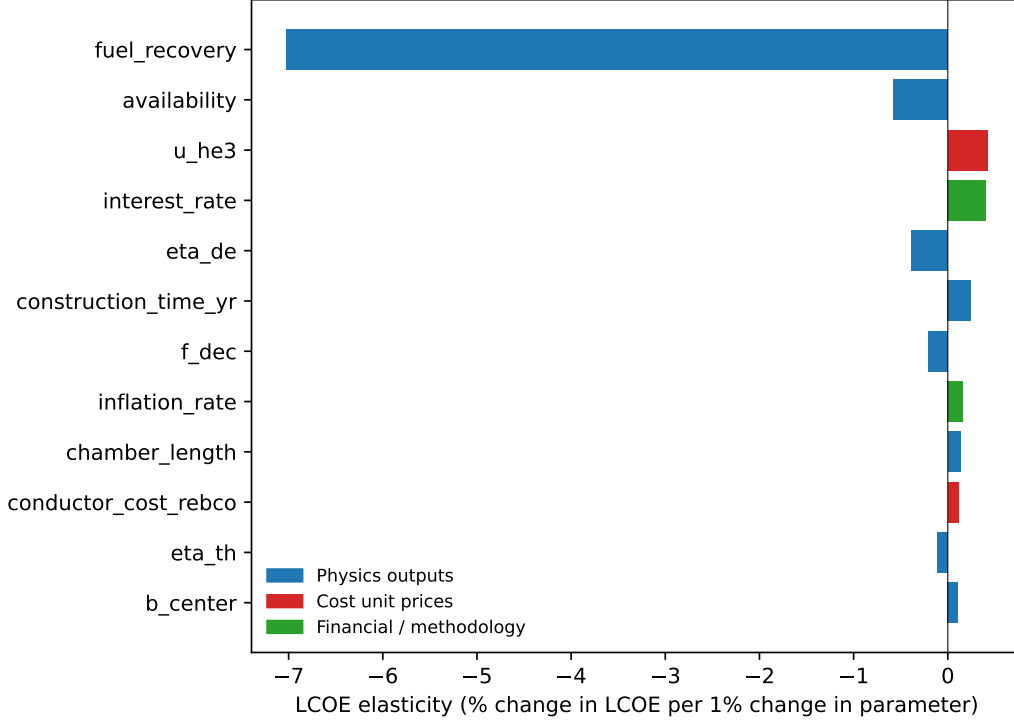


Figure 2: Sensitivity tornado for the 1 GWe D-³He mirror reference scenario. Bars give LCOE elasticity $\epsilon_p = (\partial \text{LCOE} / \partial p)(p / \text{LCOE})$ computed by reverse-mode autodiff on the full forward pipeline. A bar of length 0.10 means a +1% perturbation of the parameter moves LCOE by +0.10%. Recorded by `scripts/make_tornado.py`.

improvement in `fuel_recovery` cuts fresh ³He purchases sharply. Combined with the high ³He price (`u_he3`), this explains the unusually large elasticity. The financial bucket entries are modest for this reference scenario, reflecting the relatively low capital intensity of mirror designs: `interest_rate` carries an elasticity of +0.40 and `inflation_rate` +0.16.

2.4 Other API Surfaces

The forward call of section 2.2 is the primary API entry point. Four additional API surfaces address common variants.

Costing constants. The calibration constants behind the parametric estimates (unit prices, fabrication markups, fractions) are exposed as forward keywords and can be overridden directly. For example, to test a more optimistic ³He price:

```
result = model.forward(
    net_electric_mw=1000.0, availability=0.87, lifetime_yr=30,
    u_he3=1_000_000.0, # $/kg, optimistic He-3 price
)
```

This rescales every account that consumes the constant (here CAS80, the ³He fuel cost), in contrast to a cost override, which replaces an account total outright.

Cost overrides. A vendor quote may replace a parametric estimate without re-running the physics:

```

result = model.forward(
    net_electric_mw=1000.0, availability=0.87, lifetime_yr=30,
    cost_overrides={"C220103": 436.0}, # M$, mirror coil quote
)

```

Downstream rollups (CAS22, total capital, LCOE) recompute automatically. Mirror coils are typically smaller absolute cost than tokamak TF/CS/PF systems, reflecting the simpler solenoid topology. Overrides apply to the direct-capital accounts (CAS10 and CAS21–CAS28, including individual CAS22 sub-accounts); the downstream aggregates (CAS29–CAS30), owner and supplementary costs (CAS40–CAS50), interest during construction (CAS60), and the annualized operations, fuel, and financial accounts (CAS70–CAS90) are computed from these and the physics, so they are not overridden directly. When an override is supplied at a reference power and the plant is then rescaled, only these directly-overridable accounts carry the override forward, each rescaled by its own cost ratio between the two power points.

Batch sweeps. `batch_lcoe` computes LCOE for many values of one or more parameters in a single call, returning a list of LCOE figures (in \$/MWh) aligned with the input grid. Vectorised via `vmap`, it is suitable for uncertainty-band propagation and Monte Carlo:

```

lcoes = model.batch_lcoe(
    {"dhe3_f_T": [0.3, 0.4, 0.5, 0.6, 0.7]},
    params=result.params,
)

```

The swept parameter here is the secondary D-T burn fraction, i.e. the fraction of D-D-bred tritium that goes on to fuse with deuterium. Higher values add fusion power but also raise the 14.1 MeV neutron load.

Backcasting. Solves the inverse problem: which value of a single parameter hits a target LCOE, given everything else fixed.

```

from costingfe.analysis.backcast import backcast_single
eta_de_target = backcast_single(
    model, target_lcoe=78.0, param_name="eta_de",
    param_range=(0.50, 0.85), base_params=result.params,
)

```

This example determines the venetian-blind efficiency required to bring the mirror reference plant to a 78 \$/MWh LCOE.

The remainder of this paper is a detailed report of the calculation that is being executed by the code. Section 3 formalises how annualized capital and operating costs combine into LCOE, section 4 covers the power balance and radiation physics that determine plant size and recirculating power, and section 5 describes the per-account costing methods that produce the rollout of table 2.

3 Economics Module

The levelized cost of electricity is the constant electricity price at which the present value of revenue equals the present value of all costs over the plant lifetime. It aggregates annualized capital and operating costs into a single metric in \$/MWh:

$$\text{LCOE} = \frac{\text{Annualized cost}}{\text{Annual electricity production}} \quad (1)$$

The annualized cost is the sum of annualized capital cost C_{annual} and annualized operating cost M_{annual} (maintenance, fuel, and manpower), both in M\$/yr. The annual electricity production is:

$$E_{\text{annual}} = 8760 \times P_{\text{net}} \times n_{\text{mod}} \times f_{\text{avail}} \quad [\text{MWh/yr}] \quad (2)$$

where P_{net} is the net electric power per module in MW, n_{mod} is the number of reactor modules, f_{avail} is the plant availability (capacity factor), and 8760 is the number of hours per year. The computation of P_{net} from fusion power and engineering coefficients is described in the physics module (section 4). The default availability is 0.85 for all concepts (ARIES heritage); explicit values supplied at call time override this default.

Figure 3 illustrates the cash-flow structure. Total capital expenditure (CAPEX) is disbursed during the construction period, after which revenue from electricity sales and annual operating expenditure (OPEX) flow in opposite directions over the plant lifetime. OPEX is stated in base-year dollars and levelized to a constant annual charge over the plant life; because that levelization applies to the operating accounts, its procedure is given with them in section 5.14.

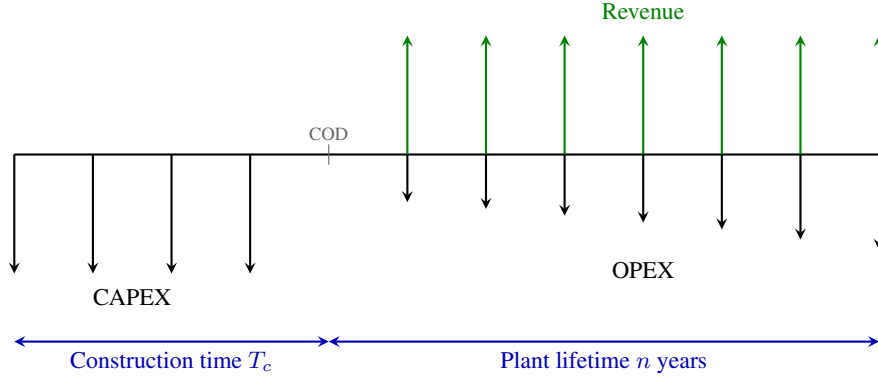


Figure 3: Schematic cash-flow diagram for a fusion power plant. Capital expenditure (CAPEX) is disbursed uniformly during the construction period T_c , accruing interest until the commercial operation date (COD). After COD, revenue from electricity sales and annual operating expenditure (OPEX) flow over the plant operating lifetime of n years. OPEX grows in nominal terms at the inflation rate. The LCOE (eq. (1)) is the constant electricity price at which the present value of revenue equals the present value of all costs.

3.1 Capital Recovery Factor

The Capital Recovery Factor (CRF) converts a present-value capital investment into equal annual payments over the plant lifetime:

$$\text{CRF}(i, n) = \frac{i(1+i)^n}{(1+i)^n - 1} \quad (3)$$

where i is the weighted-average cost of capital (WACC) and n is the plant operating lifetime in years. At reference conditions ($i = 0.07$, $n = 30$ yr), $\text{CRF} = 0.0806$.

3.2 Annualized Capital Cost

Capital expenditure is disbursed over the construction period T_c before any revenue is generated (fig. 3). Assuming the overnight capital cost C is spent in T_c equal annual installments of C/T_c , each installment accrues compound interest from the time it is spent until the commercial operation date (COD). The future value of this series at COD is:

$$\text{FV} = \frac{C}{T_c} \sum_{k=0}^{T_c-1} (1+i)^k = \frac{C}{T_c} \cdot \frac{(1+i)^{T_c} - 1}{i} \quad (4)$$

The interest during construction (IDC) is the excess above the overnight cost, the total financing charge incurred while the plant earns no revenue:

$$\text{IDC} = \text{FV} - C = C \left[\frac{(1+i)^{T_c} - 1}{iT_c} - 1 \right] \quad (5)$$

The total capital investment at COD is therefore $C + \text{IDC} = \text{FV}$, and the annualized capital cost is:

$$C_{\text{annual}} = \text{CRF}(i, n) \times (C + \text{IDC}) \quad (6)$$

At reference conditions ($i = 0.07$, $T_c = 6$ yr), the IDC adds 19.2% to the overnight cost.

4 Physics Module

The denominator of the LCOE, eq. (1), is the annual saleable electricity, which depends on the net electric power delivered to the grid P_{net} (gross output minus in-plant recirculation; eq. (28)) and plant availability. The physics module is the plant power balance for a given fuel cycle: it relates the fusion power and the net electric power by tracking the energy flow from the plasma to the grid, net of recirculating power. The fusion power itself, set by device geometry and plasma parameters, comes from a concept-specific physics model external to `1costingfe` (the user’s own, possibly proprietary, code). A computation of the plant availability would also fit in this, or an Engineering module, but requires a dedicated model incorporating the specifics of a design (e.g. maintainability, accessibility, component failure modes).

The power balance section of the physics module computes P_{net} from the fusion power P_{fus} for the four fusion fuels by tracking every energy channel from the plasma to the grid: energy split between fusion ash and neutrons, radiation losses, blanket multiplication, thermal and direct energy conversion, and recirculating power.

Many concepts will deviate significantly from the defaults; a non-Maxwellian deuterium plasma may alter the burn rates of the secondary D-D reactions, or a plasma with seeded impurities may alter the radiation losses or the plasma optical thickness [7]. These and other coefficients are therefore exposed as first-class parameters amenable to sensitivity analysis via automatic differentiation.

Given P_{fus} , the conversion to P_{net} tracks the same energy channels for any confinement scheme; the only distinction is whether the power is delivered continuously or per shot. Section 4.2 covers the steady-state balance, used for concepts such as tokamaks, stellarators, and mirrors, and section 4.3 the per-pulse balance, used for concepts such as laser IFE, Z-pinch, and pulsed inductive machines. The fusion-power split (section 4.1) is upstream of both.

4.1 Fusion Power Split

Operating the power plant requires collecting the power leaving the plasma and converting it to electricity. The fusion reaction releases energy as charged particles and neutrons; the split between these two channels is set by the nuclear physics of the fuel cycle. Neutrons deposit their energy volumetrically in the blanket and shielding. The charged-particle energy leaves the plasma through two channels: photon emission (bremsstrahlung, synchrotron, and line radiation), governed by plasma physics rather than nuclear kinematics and treated separately in section 4.2; and direct charged-particle transport to plasma-facing surfaces. Most of this energy is converted to electricity via a thermal cycle, though a fraction of the charged-particle transport loss may be recovered directly via direct energy conversion (DEC) systems.

The purpose of this calculation is to determine the charged-particle and neutron power split. The neutron energy fraction $f_n \equiv E_n/Q$, where Q is the total energy released by the primary reaction and E_n is the portion carried by neutrons. For fuel cycles with secondary burns (D-D, D- ^3He), f_n is generalised to $\bar{E}_n/\bar{E}_{\text{total}}$ using the effective averages defined in the subsections below. Table 3 summarizes the primary reaction for each fuel cycle:

Table 3: Primary fusion reaction by fuel cycle.

Fuel	Q (MeV)	f_n	Products
D-T	17.6	0.80	$^4\text{He} + \text{n}$
D-D	3.65	0.33	$\begin{cases} ^3\text{He} + \text{n} \\ \text{T} + \text{p} \end{cases}$
D- ^3He	18.3	0.0	$^4\text{He} + \text{p}$
p- ^{11}B	8.7	0.0	3^4He

A complementary fuel-cycle quantity is the *single-pass burn fraction* f_b (`burn_fraction`; sometimes called injection burnup): the fraction of fuel atoms injected into the plasma that undergo fusion before being exhausted. For magnetic confinement at reactor-relevant densities and confinement times, f_b of order 1–10%. Unburned fuel is exhausted, separated, and recycled with efficiency f_r (`fuel_recovery`); the resulting cumulative fusion probability of an injected

atom is $f_b/[1 - f_r(1 - f_b)]$, approaching 1 as $f_r \rightarrow 1$. Both f_b and f_r are used in CAS80 (section 5.13). Both are declared per-concept in the engineering YAMLS rather than as global defaults, with the NOAK $f_r = 0.99$ uniform across concepts. Per-concept values and provenance are given in appendix D.

4.1.1 Deuterium-tritium (D-T)

The D-T reaction is the simplest case: each fusion event releases a fixed $Q = 17.6$ MeV, split by momentum conservation into a 3.5 MeV alpha particle and a 14.1 MeV neutron ($f_n = 0.80$). The alpha ash (^4He) is inert and does not undergo further reactions, so the power split is fully determined by the primary kinematics.

4.1.2 Deuterium-deuterium (D-D)

The D-D fuel cycle branches into two channels with approximately equal probability, producing either tritium and a proton (branch 1) or ^3He and a neutron (branch 2). The tritium and ^3He products are themselves fusion fuels that react with the majority species of deuterium in the plasma. The deuterium-tritium (D-T) reaction has a much higher cross section than the D-D reaction, so the tritium from branch 1 undergoes secondary D-T fusion with a burn fraction f_T (dd_f_T) that approaches 1 at typical D-D burn temperatures. The D- ^3He reaction has a cross section comparable to D-D, so the ^3He product from branch 2 undergoes secondary D- ^3He fusion with a burn fraction $f_{^3\text{He}}$ (dd_f_He3) that is typically lower than f_T .

The effective energy per D-D event, and the split between charged particles and neutrons, is determined by the burn fractions of these secondary reactions. The burn fractions depend on the plasma conditions and confinement time, and are currently treated as free parameters in the framework, with default values informed by typical D-D burn conditions in the literature [8]. A detailed plasma model could be added to compute these burn fractions from plasma parameters and replace the defaults. The effective energy per D-D event, averaged over the two primary branches, becomes:

$$\bar{E}_{\text{total}} = \frac{1}{2}(Q_1 + Q_2) + \frac{1}{2}f_T Q_{\text{DT}} + \frac{1}{2}f_{^3\text{He}} Q_{\text{D}^3\text{He}} \quad (7)$$

where $Q_1 = 4.03$ MeV and $Q_2 = 3.27$ MeV are the primary branch Q-values. Each secondary reaction consumes one additional deuteron, so the total deuterons consumed per primary D-D event is $2 + \frac{1}{2}f_T + \frac{1}{2}f_{^3\text{He}}$. The neutron energy per primary D-D event is

$$\bar{E}_n = \frac{1}{2}E_{n,1} + \frac{1}{2}f_T E_{n,\text{DT}} \quad (8)$$

where $E_{n,1} = 2.45$ MeV is the neutron from primary branch 2 and $E_{n,\text{DT}} = 14.1$ MeV is the neutron from the secondary D-T reaction; the secondary D- ^3He reaction produces only charged particles and contributes no neutrons. At default burn fractions ($f_T = 0.97$, $f_{^3\text{He}} = 0.69$), 2.83 deuterons are consumed per primary event, the effective total energy rises from 3.65 MeV to approximately 18.5 MeV, and the effective neutron energy fraction $\bar{E}_n/\bar{E}_{\text{total}}$ increases from 0.33 to approximately 0.44 due to the secondary D-T neutrons.

4.1.3 Deuterium-helium 3 (D- ^3He)

The D- ^3He fuel cycle is the most complex of the four considered here: the primary reaction is aneutronic ($Q = 18.3$ MeV), but at the required temperatures ($T_i = 60\text{--}100$ keV) a fraction f_{DD} (dhe3_dd_frac) of fusion events are D-D side reactions, which themselves carry the D-T and D- ^3He secondaries described in the D-D section above. The D-D events produce tritium (via D(d,p)T) that re-burns in D-T fusion at a concept-specific burn fraction f_T^* (dhe3_f_T), introducing 14.1 MeV neutrons into an otherwise neutron-free system. They also produce ^3He (via D(d,n) ^3He) that re-burns in D- ^3He fusion at burn fraction $f_{^3\text{He}}^*$, releasing additional charged-particle energy and reducing the external ^3He demand of the plant.

The effective total energy and neutron energy per D- ^3He event are:

$$\bar{E}_{\text{total}} = Q_{\text{D}^3\text{He}} + f_{\text{DD}} \bar{E}_{\text{total,DD}} \quad (9)$$

$$\bar{E}_n = f_{\text{DD}} \bar{E}_{n,\text{DD}} \quad (10)$$

where $\bar{E}_{\text{total,DD}}$ follows the structure of eq. (7) including both secondary burns:

$$\bar{E}_{\text{total,DD}} = \frac{1}{2}(Q_1 + Q_2) + \frac{1}{2}f_T^* Q_{\text{DT}} + \frac{1}{2}f_{^3\text{He}}^* Q_{\text{D}^3\text{He}}$$

and $\bar{E}_{n,DD}$ follows eq. (8): only the D-T secondary burn contributes neutrons, since the secondary D- ^3He reaction is aneutronic.

The bred-tritium burn fraction f_T^* is a design choice: burn for energy or exhaust to reduce the neutron load. Mirror plants without active tritium discharge let bred T burn at $f_T^* \approx 0.5$ (single-pass thermal burn); pulsed FRC architectures designed for low neutron load may exhaust (or hold for decay) bred tritium, giving $f_T^* \approx 0$.

The bred- ^3He utilization $f_{^3\text{He}}^*$ is not a free parameter: bred ^3He is chemically identical to primary ^3He and enters the same exhaust/recovery loop. Its cumulative fusion probability equals that of primary ^3He ,

$$f_{^3\text{He}}^* = \frac{f_b}{1 - f_r(1 - f_b)}, \quad (11)$$

where f_b is the single-pass burn fraction (burn_fraction) and f_r the fuel recovery (fuel_recovery), both introduced in section 5.13. The framework computes it automatically. With representative MFE-class values $f_b = 0.05$ and $f_r = 0.99$, $f_{^3\text{He}}^* \approx 0.84$; concept-specific values flow through from the per-concept YAMLs.

Per primary D- ^3He event, the deuteron consumption is $1 + f_{DD}(1 + \frac{1}{2}f_T^* + \frac{1}{2}f_{^3\text{He}}^*)$ and the external ^3He consumption is $(1 - f_{DD}) - \frac{1}{2}f_{DD}f_{^3\text{He}}^*$, the latter accounting for D-D-bred ^3He that re-burns in place of an external atom. For the steady-state mirror concept evaluated at $f_{DD} = 0.131$ (50/50 D/ ^3He mix at $T_i = 70$ keV with Bosch-Hale cross sections [9]), $f_T^* = 0.5$, and the default $f_{^3\text{He}}^* \approx 0.84$ (from eq. (11)), the effective neutron energy fraction $\bar{E}_n/\bar{E}_{\text{total}}$ is approximately 3%, small but nonzero, and consequential for shielding, activation, and tritium breeding requirements. The link between f_{DD} , the D/ ^3He density ratio, and operating temperature follows from the reaction-rate ratio:

$$f_{DD} = \frac{\langle\sigma v\rangle_{DD}(T_i)}{\langle\sigma v\rangle_{DD}(T_i) + 2(n_{^3\text{He}}/n_D)\langle\sigma v\rangle_{D^3\text{He}}(T_i)}, \quad (12)$$

where the factor of 2 accounts for the identical-particle reduction of the D-D rate.

4.1.4 Proton-boron 11 (p- ^{11}B)

The primary p- ^{11}B reaction produces three alpha particles ($Q = 8.7$ MeV) with a broad energy spectrum. Dmitriev [10] reports a primary alpha peaking near 4.5 MeV and two secondary alphas from the decay of an excited ^8Be intermediate at approximately 2.4 MeV each. These alphas are not inert ash but can undergo further reactions with the boron fuel. The dominant side reaction is $^{11}\text{B}(\alpha, n)^{14}\text{N}$ ($Q = 0.16$ MeV). The Coulomb barrier between α and ^{11}B is 3.2 MeV, which is below the primary alpha energy but above the secondary alpha energies. Measured total cross sections range from 20 to 240 mb over alpha energies of 2–6 MeV, with significant resonance structure [11]. A secondary side reaction, $^{11}\text{B}(p, n)^{11}\text{C}$ ($Q = -2.76$ MeV, threshold 3.02 MeV), is endothermic and accessible to protons in the high-energy tail at a much lower rate (10^{-5} relative to the primary reaction) [12].

The framework parameterizes these via $f_{\alpha n}$ (probability per alpha of undergoing (α, n)) and f_{pn} (fraction of primary events that instead undergo (p, n)). Since each primary event produces three alphas, the effective energies per primary event are:

$$\bar{E}_{\text{total}} = Q_{pB} + 3f_{\alpha n} Q_{\alpha n} + f_{pn} Q_{pn} \quad (13)$$

$$\bar{E}_n = 3f_{\alpha n} E_{n,\alpha} + f_{pn} E_{n,p} \quad (14)$$

where $Q_{\alpha n} = +0.16$ MeV and $Q_{pn} = -2.76$ MeV are the side-reaction Q-values, $E_{n,\alpha} \approx 2.2$ MeV and $E_{n,p} \approx 0.17$ MeV are the neutron kinetic energies from center-of-mass kinematics. Both $f_{\alpha n}$ and f_{pn} default to zero: Ochs et al. [13] show that viable p- ^{11}B reactors must remove alpha ash on timescales much shorter than the energy confinement time to avoid excessive bremsstrahlung losses, which drastically reduces the population of MeV-scale alphas coexisting with the boron fuel and thus suppresses the dominant $^{11}\text{B}(\alpha, n)^{14}\text{N}$ channel [14]. At the default values, p- ^{11}B is treated as purely aneutronic.

4.2 Steady-State Power Balance

The steady-state balance applies to confinement concepts with continuous heating power and continuous fusion output (tokamaks, stellarators, mirrors, steady-state FRCs, levitated dipoles, polywells, and orbitrons). It converts the fusion-power split of section 4.1 into net electric power via the thermal and electric conversion stack and the recirculating-power accounting.

4.2.1 Thermal and Electric Power

The power deposited in the plasma (charged-particle fusion products P_{cp} plus external heating P_{in}) exits as radiation losses (bremsstrahlung, synchrotron, and impurity line radiation) and transport power deposited on plasma-facing surfaces. Bremsstrahlung power [15]:

$$P_{brem} = 5.35 \times 10^{-37} n_e^2 Z_{eff} \sqrt{T_e} V \quad [\text{W}] \quad (15)$$

where n_e is the electron density in m^{-3} , T_e the volume-averaged electron temperature in keV, Z_{eff} the effective charge, and V the plasma volume in m^3 . Equation (15) is the non-relativistic electron-ion form, accurate at the D-T and D-D operating temperatures (T_e of order 10–30 keV), and it is applied (summed with synchrotron and impurity-line radiation below) only for those two fuels. At the high temperatures of the aneutronic fuels ($\text{D-}^3\text{He}$ and $\text{p-}^{11}\text{B}$, $T_e \gtrsim 100$ keV) relativistic and electron-electron bremsstrahlung corrections become significant and the thermal synchrotron estimate breaks down, so the framework does not apply these formulas to $\text{D-}^3\text{He}$ or $\text{p-}^{11}\text{B}$. It instead pins the radiated fraction of fusion power through `f_rad_fus`, defaulting to 0.24 for $\text{D-}^3\text{He}$ [16] and 0.83 for $\text{p-}^{11}\text{B}$ [17] (`f_rad_fus_dhe3`, `f_rad_fus_pb11`); equivalently, a fixed total radiation power can be pinned with `p_rad_override`. Either replaces the computed bremsstrahlung-plus-synchrotron-plus-impurity sum.

For synchrotron radiation, the optically thin (Larmor) formula grossly overestimates the net loss in MFE plasmas because most emission is reabsorbed. The framework uses the global model of Albajar et al. [18] with the wall-reflectivity correction of Fidone et al. [19]:

$$P_{sync} = 3.84 \times 10^{-8} C(R_w) R a^{1.38} \kappa^{0.79} B^{2.62} n_{e0,20}^{0.38} T_{e0} (16 + T_{e0})^{2.61} K G \quad [\text{MW}] \quad (16)$$

where T_{e0} and $n_{e0,20}$ are central values (keV and 10^{20} m^{-3}), R the major radius, a the minor radius, κ the elongation, and B the toroidal field in T. The correction factor $C(R_w) = (1 - R_w)^{0.62} [1 + 0.12 T_{e0} (1 - R_w)^{0.41} / p_{a0}^{0.41}]^{-1.51}$ captures wall reflectivity R_w and optical thickness via $p_{a0} = 6.04 \times 10^3 a n_{e0,20} / B$. The profile shape factor $K(\alpha_n, \alpha_T, \beta_T)$ and aspect-ratio correction $G(A) = 0.93 [1 + 0.85 e^{-0.82 A}]$ account for profile peaking and toroidal geometry. Although derived for tokamak geometry, the formula is applied to all MFE concepts: for stellarators the toroidal geometry is directly analogous, while for mirrors the effective major radius is set to $R_{eff} = L / (2\pi)$ (mapping the cylinder length L to a torus of equivalent volume) with reduced wall reflectivity to account for the open ends. IFE and MIF set $P_{rad} = 0$.

The Albajar model assumes a thermal (Maxwell–Jüttner) electron distribution. At the high temperatures required for aneutronic fuels ($T_e \gtrsim 100$ keV), synchrotron drag itself suppresses the high-energy electron tail, which is responsible for most of the emission at optically thin harmonics [20]. This self-consistent kinetic effect can reduce the net synchrotron loss by up to an order of magnitude relative to the thermal prediction. For such regimes the Albajar formula is bypassed with a kinetic Fokker–Planck radiation estimate supplied through the `p_rad_override` parameter introduced above.

Impurity Line Radiation. In MFE plasmas, line radiation from partially ionized impurities is often the dominant radiation loss channel. The framework models this via a steady-state sputtering–transport chain connecting the first-wall material to the core impurity concentration and radiative loss.

The wall material is specified as one of six options: tungsten (W), carbon (C), beryllium (Be), molybdenum (Mo), silicon carbide (SiC), or liquid lithium (Li). For each material, a simplified Bohdanský physical sputtering yield [21, 22] gives the number of wall atoms released per incident ion at the sheath-accelerated energy $E_{ion} \approx 3 T_{edge}$:

$$Y(E) = Q \left(1 - \left(\frac{E_{th}}{E} \right)^{2/3} \right) \left(1 - \frac{E_{th}}{E} \right)^2 \quad (17)$$

where E_{th} is the material-dependent threshold energy and Q is an effective fit coefficient that absorbs the Thomas–Fermi nuclear stopping cross-section $S_n(\epsilon)$. Below threshold ($E < E_{th}$), $Y = 0$. The steady-state impurity fraction in the core is then:

$$f_z = Y(3 T_{edge}) \cdot \frac{A_{fw}}{V} \cdot \frac{\tau_{imp}}{\tau_E} \cdot f_{screen} \quad (18)$$

where A_{fw}/V is the first-wall area to plasma volume ratio, τ_{imp}/τ_E is the impurity-to-energy confinement time ratio (default 3.0), and f_{screen} is the scrape-off layer screening factor (default 0.01 for high- Z materials, 0.1 for low- Z). Lithium is a special case: as a fully ionized species above 0.1 keV, it produces negligible line radiation at reactor core temperatures; the primary benefit of a liquid Li wall is low sputtering yield from continuous surface renewal and correspondingly low f_{screen} .

Deliberately seeded impurities (e.g. neon, argon) for divertor radiation or edge cooling can be specified directly via their concentration f_z , bypassing the sputtering model.

The impurity line radiation power uses coronal-equilibrium radiative loss rate coefficients $L_z(T_e)$ [23, 24], represented as piecewise power-law fits for each species:

$$P_{line} = n_e^2 \sum_z f_z L_z(T_e) V \quad [\text{W}] \quad (19)$$

The summation runs over all impurity species (both wall-derived and seeded). Cooling curves are tabulated for W, C, Be, Mo, Si, Li, Ne, and Ar.

All new parameters default to no-op values (null wall material, empty seeded impurities), preserving backward compatibility: when no wall material is specified, $P_{line} = 0$ and the radiation model reduces to bremsstrahlung plus synchrotron as before.

Plasma Energy Balance. The total radiated power is

$$P_{rad} = f_{peak} (P_{brem} + P_{line}) + P_{sync}, \quad (20)$$

computed at the user-specified electron temperature T_e . The collisional terms (bremsstrahlung and line radiation) evaluate the local emissivity $\propto n_e^2 \sqrt{T_e}$ from volume-averaged n_e and T_e and integrate it over the full geometric volume V . For a highly peaked profile this over-counts the loss, because the emission is concentrated in a small dense, hot core; the peaking factor f_{peak} rescales these terms to the emission-measure-weighted volume. Uniform-profile concepts use $f_{peak} = 1$, while a levitated dipole with a Hasegawa–Mauel core ($n_e \propto R^{-4}$, $T_e \propto R^{-8/3}$) uses $f_{peak} \approx 0.05$, the hot, dense core being about 5% of the geometric volume. Synchrotron radiation is excluded from the rescaling because the Albajar model already carries the profile dependence through the shape factor $K(\alpha_n, \alpha_T, \beta_T)$. In steady state, the plasma energy balance requires that all power entering the plasma (charged-particle fusion products plus external heating) equals all power leaving (radiation plus transport to plasma-facing surfaces):

$$P_{cp} + P_{in} = P_{rad} + P_{transport} \quad (21)$$

where P_{cp} is the charged-particle (ash) power and P_{in} is the external heating power. The transport power is therefore $P_{transport} = P_{cp} + P_{in} - P_{rad}$.

If P_{rad} exceeds $P_{cp} + P_{in}$ at the specified T_e , the user-supplied heating power is insufficient to sustain the plasma against radiation losses. Rather than capping P_{rad} implicitly (which would mask an unphysical operating point), the framework increases the effective heating power to the minimum needed to close the energy balance:

$$P_{in,eff} = \max(P_{in}, P_{rad} - P_{cp}) \quad (22)$$

This ensures $P_{transport} \geq 0$ and correctly penalizes radiation-dominated regimes through increased recirculating power: the additional heating must be supplied at wall-plug efficiency η_{pin} , which raises the recirculating power P_{recirc} (eq. (26)) and degrades the engineering Q . For example, p-¹¹B radiates a large fraction of its fusion power and so requires a large heating power; if that power is under-specified, eq. (22) scales the effective heating up to close the energy balance. That heating is recirculated at η_{pin} , raising P_{recirc} and the LCOE accordingly.

Thermal and Electric Conversion. Neutron power is absorbed in the breeding blanket, where nuclear reactions (primarily ⁶Li(n, α)T) release additional energy characterized by the blanket multiplication factor M_n (typically 1.1 for lithium blankets). The total thermal power delivered to the heat-transfer system is:

$$P_{th} = M_n P_n + P_{rad} + P_{transport} + \eta_p P_{pump} \quad (23)$$

where P_n is the neutron power, P_{rad} is the radiated power reabsorbed by the first wall, $P_{transport}$ is the charged-particle transport power deposited on plasma-facing components (eq. (21)), and $\eta_p P_{pump}$ is the fraction of pumping power

deposited as heat. The heating power P_{in} does not appear separately; it enters the plasma and exits via the radiation and transport channels already included in P_{th} . A conventional Rankine cycle with thermal efficiency η_{th} converts thermal power to gross electric power P_{et} :

$$P_{\text{et}} = \eta_{\text{th}} P_{\text{th}} \quad (24)$$

For systems with direct energy conversion (DEC), a fraction f_{dec} of the transport power bypasses the thermal cycle and is converted at efficiency η_{dec} . That fraction is removed from the thermal power of eq. (23) (only the remaining $(1 - f_{\text{dec}}) P_{\text{transport}}$ is converted thermally), so the gross electric power becomes

$$P_{\text{et}} = \eta_{\text{th}} (P_{\text{th}} - f_{\text{dec}} P_{\text{transport}}) + f_{\text{dec}} \eta_{\text{dec}} P_{\text{transport}}. \quad (25)$$

f_{dec} is a per-concept default: zero for tokamaks, stellarators, dipoles, and steady-state FRCs, and nonzero where charged-particle exhaust is naturally collected (0.3 for mirrors, 0.5 for polywells, 0.9 for orbitrons).

4.2.2 Recirculating Power and Net Electric Output

A fraction of the gross electric power P_{et} is recirculated to sustain the plant:

$$P_{\text{recirc}} = \frac{P_{\text{in,eff}}}{\eta_{\text{pin}}} + P_{\text{coils}} + P_{\text{pump}} + P_{\text{cryo}} + P_{\text{cool}} + f_{\text{sub}} P_{\text{et}} + P_{\text{other}} \quad (26)$$

where $P_{\text{in,eff}}/\eta_{\text{pin}}$ is the wall-plug power for the heating system (using the effective heating power from eq. (22)), P_{coils} powers the magnets, P_{cryo} and P_{cool} serve the cryogenic and cooling systems, $f_{\text{sub}} P_{\text{et}}$ covers balance-of-plant subsystems (typically 3%), and P_{other} includes tritium processing and housekeeping loads.

The heating wall-plug efficiency is not a single device constant but a product of a method-level source efficiency and a device-level coupling efficiency,

$$\eta_{\text{pin}} = \frac{\sum_i P_i}{\sum_i P_i / (\eta_{\text{src}}(i) \eta_{\text{cpl}})}, \quad (27)$$

where i runs over the heating methods (NBI, ICRF, ECRH, LHCD) in the mix, $\eta_{\text{src}}(i)$ is the wall-plug-to-delivered source efficiency of method i (negative-ion NBI 0.60, ICRF 0.70, ECRH 0.50, LHCD 0.50), and η_{cpl} is the concept's delivered-to-absorbed coupling. As a result, the recirculating heating load reflects the actual driver: a beam-driven FRC, whose tangential injection through long ducts and short plasma path give a coupling of only $\eta_{\text{cpl}} \approx 0.43$ (C-2W), yields $\eta_{\text{pin}} = 0.60 \times 0.43 = 0.26$, whereas an RF-driven device couples substantially more efficiently. Concepts whose input power is not delivered by an NBI/RF heating system (electrostatic confinement; pulsed drivers) specify η_{pin} directly. The per-concept η_{cpl} values are chosen so the product reproduces each benchmarked concept's calibrated η_{pin} , leaving the benchmarks unchanged while making the method-dependence explicit.

The net electric power is:

$$P_{\text{net}} = P_{\text{et}} - P_{\text{recirc}} \quad (28)$$

The engineering gain $Q_{\text{eng}} = P_{\text{et}}/P_{\text{recirc}}$ must exceed unity for the plant to produce net electricity. The recirculating fraction $1/Q_{\text{eng}}$ is a key figure of merit: lower recirculating fractions leave more power for sale and directly reduce the LCOE denominator.

The inverse-balance solver used by the costing model is presented in appendix C.

4.3 Pulsed Power Balance

Pulsed confinement concepts (laser IFE, Z-pinch, and inductive recovery schemes) differ from the steady-state balance above in two respects: (i) energy is delivered in discrete pulses rather than as continuous heating, and (ii) an inductive recovery option captures the per-pulse PdV work of the expanding plasmoid directly in the driver coils, returning part of the driver energy that a thermal cycle would charge entirely as recirculating loss. `1costingfe` provides two pulsed power balance variants, selected by the `PulsedConversion` parameter.

4.3.1 Per-Pulse Energy Framework

As in the steady-state balance, the per-pulse energy is traced from the driver through to the grid. A driver delivers E_{drv} (MJ) per pulse, drawn from stored energy $E_{\text{stored}} = E_{\text{drv}}/\eta_{\text{pin}}$, where η_{pin} is the pulsed-driver wall-plug efficiency (laser, ion beam, capacitor bank; distinct from the auxiliary-heating η_{pin} of eq. (26), which decomposes into source and coupling factors). Each pulse releases fusion energy at scientific gain $Q_{\text{sci}} = P_{\text{fus}}/P_{\text{drv}}$, so the fusion power is $P_{\text{fus}} = Q_{\text{sci}} P_{\text{drv}}$ with the average driver power $P_{\text{drv}} = E_{\text{drv}} f_{\text{rep}}$ at repetition rate f_{rep} (Hz). The charged-particle fraction f_{cp} is derived from the fuel type and sets the ash–neutron split, while f_{rad} is the fraction of ash power radiated during the burn, so $P_{\text{rad}} = f_{\text{rad}} P_{\text{cp}}$. This single parameter replaces the mechanistic bremsstrahlung, synchrotron, and impurity-line radiation calculation used in the steady-state balance (section 4.2); pulsed plasmas have rapidly evolving density and temperature profiles that make the steady-state formulas inapplicable. The conversion stack below then gives the gross electric power P_{et} , and after the recirculating driver and auxiliary loads the net power $P_{\text{net}} = P_{\text{et}} - P_{\text{recirc}}$ and the engineering gain $Q_{\text{eng}} = P_{\text{et}}/P_{\text{recirc}}$ follow.

For costing the framework runs this balance inverse (as in the steady-state case): the user supplies the target net power P_{net}^* , the engineering gain Q_{eng} , and f_{rep} , and the model solves for E_{drv} and P_{fus} . Q_{eng} is taken as a primary input rather than derived because it directly determines economic viability ($Q_{\text{eng}} \leq 1$ means no net power; $Q_{\text{eng}} \approx 2$ means 50% recirculation) and works uniformly across thermal and DEC conversion pathways without requiring concept-dependent parameterization.

4.3.2 Pulsed Thermal Conversion

For laser IFE, Z-pinch, mag-target, and other pulsed concepts in which the energy leaving the plasma is absorbed as heat and converted through a thermal cycle (rather than recovered electromagnetically, as in the inductive case below), the model supports an optional partial direct charged-particle capture path that mirrors the steady-state hybrid balance of eq. (23). A fraction $f_{\text{dec}} \in [0, 1]$ of the non-radiated charged-particle power $P_{\text{ch,net}} = (1 - f_{\text{rad}}) P_{\text{cp}}$ is collected at efficiency η_{de} ; the remainder of the ash and all of the radiation thermalise into the blanket alongside the driver and pump loads:

$$P_{\text{th}} = M_n P_n + (1 - f_{\text{dec}}) P_{\text{ch,net}} + P_{\text{rad}} + P_{\text{drv}} + \eta_p P_{\text{pump}}, \quad (29)$$

$$P_{\text{dee}} = f_{\text{dec}} \eta_{\text{de}} P_{\text{ch,net}}, \quad (30)$$

$$P_{\text{et}} = \eta_{\text{th}} P_{\text{th}} + P_{\text{dee}}. \quad (31)$$

Setting $f_{\text{dec}} = 0$ recovers the pure-thermal limit in which all ash thermalises; setting it near unity for a low-neutron fuel approaches the aneutronic direct-conversion limit. The default p-¹¹B dense plasma focus uses $f_{\text{dec}} = 0.90$, modelling the LPP Fusion design that direct-converts the emitted ion beam in a decelerator [25]; the model captures this charged-particle recovery but not the separate photoelectric recovery of the X-ray power, which still thermalises. The full driver draw $P_{\text{drv}}/\eta_{\text{pin}}$ still enters the recirculating load; unlike the inductive case below, the thermal-mode driver charge is not recovered.

4.3.3 Pulsed Inductive DEC Conversion

For pulsed concepts in which the plasma’s expansion energy is recovered electromagnetically rather than as heat (the pulsed FRC, e.g. Helion, and the theta pinch), the framework includes a dedicated inductive direct-energy-conversion model. The driver energy circulates in an electromagnetic loop (capacitor bank → compression coils → plasma → coils → capacitor bank). The compressed plasma fuses, and the charged-particle ash expands, doing PdV work on the magnetic field, which induces current back into the coils. The fraction of net charged-particle power that couples as PdV work, for plasma expanding adiabatically from r_{min} to r_{max} , is

$$f_{\text{pdv}} = 1 - \left(\frac{r_{\text{min}}}{r_{\text{max}}} \right)^{2(\gamma-1)} \quad (32)$$

with $\gamma = 5/3$ for an ideal monatomic plasma. The recovered and net DEC powers are then

$$P_{\text{recovered}} = \eta_{\text{dec}} (P_{\text{drv}} + f_{\text{pdv}} P_{\text{ch,net}}), \quad (33)$$

$$P_{\text{dee}} = P_{\text{recovered}} - P_{\text{drv}}, \quad (34)$$

where $P_{\text{ch,net}} = (1 - f_{\text{rad}}) P_{\text{cp}}$ and η_{dec} is the round-trip efficiency of the inductive recovery circuit.

A key distinction from the steady-state balance is the recirculating load: because the capacitor bank energy goes out and comes back each cycle, only the charging losses $P_{\text{drv}} (1/\eta_{\text{pin}} - 1)$ are drawn from the grid, not the full $P_{\text{drv}}/\eta_{\text{pin}}$.

Neutrons, bremsstrahlung, and undirected charged particles still enter a thermal blanket. When $\eta_{th} > 0$ a conventional thermal cycle runs in parallel with the DEC, and the total gross electric is $P_{et} = P_{dec} + P_{the}$. When $\eta_{th} = 0$ the concept is purely inductive, and that thermal power is dumped as waste heat rather than converted to electricity.

For the DEC inverse, the model takes the scientific gain Q_{sci} as input and derives the required stored energy per pulse:

$$E_{stored} = \frac{P_{net}}{f_{rep}(\eta_{eff}(1 + Q_{sci}f_{cp}) - 1)\eta_{pin}} \quad (35)$$

where η_{eff} combines the DEC and thermal conversion efficiencies. This ensures that higher DEC efficiency correctly reduces the required capacitor bank size rather than inflating it.

5 Cost Account Structure

The cost account structure maps the financial framework of section 3 onto specific plant systems and activities. Capital accounts CAS10–CAS60 sum to the total capital investment (CAPEX); annualized operating accounts CAS70 and CAS80 constitute OPEX; and CAS90 annualizes the CAPEX via the CRF. Table 4 shows the full hierarchy.

The *Disposition* column flags whether the account uses prior conventions unchanged (*Inherited*), keeps the prior backbone with additional sub-cases (*Extended*), or has been re-derived from procurement and first principles (*Replaced*). Here the prior conventions are the cost calculations (the heritage scaling laws) of the pyFECONS implementation [4, 5]. Subsections in this chapter present methodology only for accounts in the latter two categories.

A contingency rate f_{cont} is applied to the direct accounts (CAS10, the CAS21–28 sum via CAS29, and CAS50): $f_{cont} = 10\%$ for FOAK and 0% for NOAK, following the Gen-IV EMWG convention [3]. The 10% FOAK rate is conservative relative to the EMWG recommendation of 15–20% for advanced reactors (the CAS22 sub-accounts already carry conservative fabrication markups); the 0% NOAK rate reflects a mature, standardised design with resolved construction risk.

The following subsections detail the methodology for each account that has undergone independent review and justification.

5.1 CAS10: Pre-Construction Costs

CAS10 covers land acquisition, site and plant permits, licensing, engineering studies, and pre-construction reports. It is typically less than 1% of total capital; individual sub-accounts do not warrant detailed parametric modeling. The account is the land cost plus the fixed pre-construction items, with contingency:

$$CAS10 = (1 + f_{cont}) [C_{11} + c_{site} + C_{13} + c_{studies} + c_{permit} + c_{reports} + c_{other}], \quad (36)$$

where C_{11} is the land cost (section 5.1.1), C_{13} the fuel-dependent licensing cost (section 5.1.2), $c_{studies}$ the FOAK or NOAK engineering-study cost, the remaining c s the site-permit, plant-permit, report, and other items, and f_{cont} the contingency rate defined above. The fixed line-item values are listed in appendix A.

5.1.1 Land and Land Rights (CAS11)

The land cost scales with the square root of plant-total net electric power,

$$C_{11} = I_{land} \sqrt{P_{net} n_{mod} P_{ref} c_{land} / 10^6}, \quad (37)$$

where I_{land} is the land intensity (acres/MWe), $P_{ref} = 1000$ MWe the reference net electric power, and c_{land} the land price (\$/acre). P_{ref} is the common 1 GWe normalization at which the net-electric-scaling coefficients are calibrated; it recurs in the staffing (CAS40, CAS71) and supplementary (CAS50) accounts below. The square-root form gives a compact site whose footprint grows sublinearly with plant size, as in a gas combined-cycle station that shares one site across generating blocks, so that a 1 GWe single-module plant recovers the intensity I_{land} directly. Modern compact fusion plant designs require 20–200 acres, far less than the legacy 1,000-acre assumption in earlier ARIES studies. A representative compact pilot-plant filing [26] plans 100 acres for 400 MWe, giving a land intensity of 0.25 acres/MWe. At US industrial-zoned land costs of approximately \$10 000/acre (consistent with USDA farmland averages scaled for industrial zoning¹), land cost for a 1 GWe plant is approximately \$2.5M, negligible in the context of multi-billion-dollar capital investments.

The compact siting follows from the absence of an exclusion zone: the NRC’s 2023 decision to regulate fusion energy systems under 10 CFR Part 30 (byproduct materials) rather than Part 50/52 (reactor licensing) eliminates the large-radius emergency planning zone required for fission plants [27].

¹USDA NASS, *Land Values 2024 Summary*, August 2024.

Table 4: Cost account structure overview. Accounts with dedicated methodology subsections are marked with †.

CAS	Description	Disposition	Method
10 [†]	Pre-construction	Replaced	Land intensity scaling, fuel-dependent licensing
20	Total direct costs	–	Sum of CAS21–29
21 [†]	Buildings & structures	Replaced	Per-building, per-fuel, industrial-grade (18 buildings)
22 [†]	Reactor plant equipment	–	Component-level parametric (18 sub-accounts)
<i>Per-module accounts ($\times n_{mod}$):</i>			
22.01.01 [†]	First wall + blanket	Extended	Volume \times thermal intensity \times fuel \times blanket-form structural complexity factor
22.01.02	Shield	Inherited	Volume \times fuel-dependent neutron scale
22.01.03 [†]	Coils (magnets)	Replaced	Conductor kAm \times \$/kAm \times markup; \$0 for IFE
22.01.04 [†]	Heating (MFE) / driver (pulsed)	Extended	Per-MW heating; pulsed driver per-MJ (laser/accelerator) or per-MW (mechanical)
22.01.05	Primary structure	Inherited	Volume \times power scale
22.01.06 [†]	Vacuum system	Extended	Vessel volume scale + gas-load pumping ($S = Q/P_{op}$)
22.01.07 [†]	Power supplies	Replaced	Power-scaled (MFE); \$/J stored basis for all pulsed
22.01.08	Divertor / target factory	Inherited	Thermal-scaled (MFE) or power-scaled (IFE)
22.01.09	Direct energy converter	Replaced	Mirror/FRC model; circuit-derived markups for inductive DEC
22.01.10 [†]	Remote handling & maintenance	Replaced	Fuel- and concept-dependent
22.01.11	Installation labor	Inherited	14% of reactor subtotal
22.01.12 [†]	Isotope separation plant	Replaced	Zeroed; market purchase in CAS80
<i>Plant-wide accounts:</i>			
22.02	Main & secondary coolant	Inherited	Power-scaled
22.03	Auxiliary cooling + cryoplant	Inherited	Power-scaled + cryo load basis
22.04	Radioactive waste management	Inherited	Thermal-scaled
22.05	Fuel handling & storage	Inherited	Fuel-dependent, power-scaled (0.7)
22.06	Other reactor plant equip.	Inherited	Power-scaled (0.8)
22.07	Instrumentation & control	Inherited	Thermal-scaled (0.65)
23 [†]	Turbine plant equipment	Replaced	Linear scaling on thermal electric P_{the} (NETL-calibrated)
24 [†]	Electric plant equipment	Replaced	Linear scaling on gross electric (NETL-calibrated)
25 [†]	Miscellaneous plant equip.	Replaced	Linear scaling on gross electric (NETL-calibrated)
26 [†]	Heat rejection systems	Replaced	Linear scaling on total thermal P_{th} (NETL-calibrated)
27 [†]	Special materials	Extended	Volume-based blanket-fill inventory: $V_{blk} \times \text{vol-frac} \times \text{density} \times \text{\$/kg}$ (PbLi / Li / FLiBe / Be ceramic / ceramic only / none)
28 [†]	Digital twin	Replaced	Fixed cost (\$5M)
29 [†]	Contingency on direct costs	Inherited	10% FOAK, 0% NOAK (Gen-IV EMWG)
30 [†]	Indirect service costs	Replaced	Fraction of CAS20, construction-time scaled
40 [†]	Owner’s costs	Replaced	Fuel-dependent, staffing-based, power-law scaled
50 [†]	Supplementary costs	Replaced	Fuel-dependent sub-account model (6 components)
60 [†]	Interest during construction	Inherited	Uniform-spending IDC formula
70 [†]	Annualized O&M + replacement	Replaced	Growing-annuity levelization
80 [†]	Annualized fuel cost	Replaced	Fuel-specific consumables, burn-fraction corrected, leveled
90 [†]	Annualized financial costs	Inherited	CRF \times total capital

5.1.2 Plant Licensing (CAS13)

Licensing is fuel-dependent and enters the model two ways. A fixed licensing cost CAS13 is charged in CAS10 (eq. (36)). Separately, the licensing time $t_{\text{lic}}(f)$ extends the total project time of a first-of-a-kind (FOAK) build,

$$T_{\text{project}} = \begin{cases} T_c + t_{\text{lic}}(f) & \text{FOAK} \\ T_c & \text{NOAK,} \end{cases} \quad (38)$$

where T_c is the construction time. T_{project} is the inflation horizon T_c used in the levelized annual cost of CAS70 and CAS80 (eq. (83)); the n th-of-a-kind build incurs no licensing delay. Table 5 lists the adopted values.

Table 5: Licensing cost and timeline by fuel cycle.

Fuel	CAS13 (M\$)	t_{lic} (yr)	Rationale
D-T	5.0	2.0	Part 30 licensing, upper end of 1–2 yr range
D-D	3.0	1.5	Reduced tritium inventory
D- ³ He	1.0	0.75	Minimal radioactivity
p- ¹¹ B	0.1	0.0	No radioactivity

5.2 CAS21: Buildings and Structures

CAS21 covers all buildings and structures on the fusion plant site. Each building is priced individually per fuel type based on its physical scope and construction grade, not a blanket multiplier. Under the Part 30 regulatory basis (section 5.1), most buildings are costed at conventional industrial construction grade, with elevated radiological standards applied only to the tritium and activated-component areas.

5.2.1 Fuel and Power Scaling

Each building is costed for what it physically is, and scales with its own driver (fixed footprint, plant power, or staff), so the account is the sum

$$C_{21} = \sum_b c_b(f) \left(\frac{P_b}{P_{b,\text{ref}}} \right)^{\alpha_b}, \quad (39)$$

where $c_b(f)$ is building b 's fuel-dependent reference cost (table 7), P_b its plant-total scaling power with $P_{b,\text{ref}}$ the 1 GWe reference, and $\alpha_b \in \{0, \frac{1}{2}, 1\}$ for fixed, staff-scaled, and power-scaled buildings. The superconducting-magnet cryoplant building is included only for superconducting-coil concepts. The per-fuel totals (each a sum of the individually-costed buildings) are summarized in table 6.

Table 6: CAS21 buildings cost by fuel cycle.

Fuel	Value at 1 GWe (M\$)	Construction grade
D-T	629	Enhanced industrial (tritium confinement, hot cell, rad-HVAC)
D-D	576	Enhanced industrial (reduced tritium/activation scope)
D- ³ He	452	Light enhanced industrial
p- ¹¹ B	385	Industrial (no hot cell, no tritium, standard HVAC)

Table 7 lists each building with its per-fuel cost at the 1 GWe reference and the power quantity it scales with.

The fuel dependence is governed by activation and tritium handling: the buildings that shield neutrons or confine tritium (reactor building, hot cell, ventilation/HVAC) decline from D-T through D-³He as the neutron energy and tritium inventory fall, and the hot cell is eliminated entirely for aneutronic p-¹¹B (no material activation occurs). Ventilation scales with P_{fus} because its dominant load is confinement rad-ventilation of the reactor building, not office comfort HVAC. The cryogenics building is the magnet cryoplant, present only for superconducting-magnet concepts and zero for normal-conducting (copper) and magnet-free designs.

All power-scaling buildings are driven by *plant-total* power: when a plant is assembled from n_{mod} replicated modules, they are fed n_{mod} times the per-module power (the same total the balance-of-plant accounts CAS23–26 use), reaching plant scale rather than being pinned to a single module; fixed buildings are charged once per site.

Table 8 situates the fuel-dependent CAS21 figures of table 6 against non-fusion plant types.

Table 7: CAS21 buildings by fuel cycle and scaling driver (M\$ at the 1 GWe net reference). Fuel-independent buildings span the fuel columns.

Building	D-T	D-D	D- ³ He	p- ¹¹ B	Scales with
Reactor building	138	127	98	81	P_{fus}
Hot cell	104	78	23	0	P_{fus}
Reactor auxiliaries	29	25	21	17	P_{fus}
Ventilation/HVAC	17	15	6	3.5	P_{fus}
Site improvements	85	81	75	69	fixed
Maintenance	17	16	15	14	fixed
Control room	14	13	12	12	fixed
Fuel storage	9	7	3	1	fixed
Site services	5	5	3.5	3.5	fixed
Security	3.5	3.5	2.3	2.3	fixed
Administration	9	8	6	5	$P^{0.5}$ (staff)
Turbine building			58		P_{the}
Heat exchanger			17		P_{th}
Service water			9		P_{th}
Power supply			17		P_{et}
On-site AC			12		P_{et}
Cryogenics			14		fixed (superconducting only)
Assembly hall			21		fixed

Table 8: CAS21 buildings \$/kW benchmark comparison.

Plant type	Buildings \$/kW	Grade
Gas combined-cycle (CCGT)	150–250	Industrial
Coal (NETL B12A)	175–300	Heavy industrial
Fission nuclear (Part 50)	800–1,300	Nuclear-grade

The fusion p-¹¹B figure of 384 \$/kW corresponds to roughly $1.7 \times$ CCGT, and the D-T figure of 626 \$/kW at roughly $3.0 \times$ CCGT. The values are derived from first principles using industrial construction benchmarks [28, 29, 30].

5.3 CAS22: Reactor Plant Equipment

CAS22 (reactor plant equipment) is the largest direct-capital account and the most concept- and fuel-sensitive. Following the dispositions of table 4, several sub-accounts inherit prior scaling unchanged, while the rest (coils, supplementary heating / driver, vacuum system, power supplies, direct energy converter, remote handling, and isotope separation) are re-derived from component physics and procurement. The inherited sub-accounts are summarized first, then each re-derived account in turn.

5.3.1 Inherited Sub-Accounts

Sub-accounts CAS22.01.02 (shield), 22.01.05 (primary structure), and 22.01.11 (installation labor) inherit the methodology of the pyFECONS implementation [4] unchanged: hybrid volume + thermal-intensity scaling for component accounts and percentage-of-subtotal for installation labor. They are not re-derived here.

5.3.2 CAS22.01.01: First Wall and Blanket

Sub-account CAS22.01.01 (first wall + blanket) prices the blanket volume V_{blk} (the first-wall, blanket, and reflector volume from the geometry model) at a fuel-keyed unit cost $c_{\text{blk}}(f)$, with a power scaling and a blanket-form structural complexity factor $s(\text{form}) \in \{1.0, 1.3, 1.2, 0.0\}$ for liquid-metal, molten-salt, solid-breeder, and no-blanket architectures. The D-T unit cost is anchored to a RAFM-steel materials mass build-up at the reference machine (about 3500 t of fabricated nuclear-grade structure, breeder, and multiplier, cross-checked against the 440-module ITER blanket/shield) and priced at mature, Nth-of-a-kind unit costs:

$$C_{22.01.01} = c_{\text{blk}}(f) \cdot s(\text{form}) \cdot V_{\text{blk}} \cdot \left(\frac{P_{\text{th}}}{P_{\text{th,ref}}} \right)^{0.6} \quad (40)$$

where $P_{\text{th,ref}} = 2500$ MWth is the reference machine’s thermal power (also used for the shield, CAS22.01.02) and the 0.6 exponent captures the sublinear growth of blanket cost with thermal load at fixed volume. The structural factor represents the cassette/canister fabrication premium for molten-salt designs (Hastelloy-N corrosion liner on FLiBe-wetted surfaces) and solid-breeder designs (pebble-bed canisters with separate breeder and multiplier zones), all relative to the PbLi-style flow-channel baseline. The fill material chemistry is costed separately under CAS27 (section 5.5).

The fuel-keyed unit cost $c_{\text{blk}}(f)$ is 0.60, 0.30, 0.08, and 0.05 M\$/m³ for D-T, D-D, D-³He, and p-¹¹B, declining from a full PbLi breeding blanket (D-T: about 9.4 t/m³, with a flow loop, MHD ducts, and online tritium extraction) to a thin X-ray-capture wall with no breeding (p-¹¹B). A solid Li₂O ceramic breeder (used by the levitated dipole) has none of these, runs at about 2 t/m³, and is roughly 3–5× cheaper per unit volume, so concepts with a Li₂O fill substitute a dedicated unit cost $c_{\text{Li}_2\text{O}} = 0.2$ M\$/m³ in place of $c_{\text{blk}}(f)$.

Multi-Unit Labor Factor for $n_{\text{mod}} > 1$

Per-module installation labor (CAS22.01.11) is computed at the inherited 14% of reactor subtotal for the first unit at a site. For a multi-module site, the on-site labor for each subsequent unit is discounted by a fixed factor ϕ_{lab} :

$$C_{220111}^{\text{site}} = C_{220111}^{\text{unit } 1} \times (1 + (n_{\text{mod}} - 1) \phi_{\text{lab}}), \quad \phi_{\text{lab}} = 0.92 \text{ (default)}. \quad (41)$$

Equipment costs (CAS22.01.01–22.01.10) are *not* discounted: each module is a separate manufactured copy and incurs full equipment cost. Plant-wide accounts (CAS22.02–22.07) already use total plant power $n_{\text{mod}} P$ with sub-linear scaling exponents and capture the shared-infrastructure economy through that channel.

The factor ϕ_{lab} represents the documented twin/triplet unit co-location effect in fission EPC: re-use of construction crew, supervision, tooling, procedures, and engineering deliverables between adjacent units at a single site. The empirical anchors are roughly 20–30% labor reduction for Vogtle 3→4 (US AP1000), 10–15% across Korean APR-1400 batches (Shin-Kori, Barakah), and a smaller but positive effect on the Chinese AP1000 pairs (Sanmen, Haiyang). The European EPR pairs (Olkiluoto, Flamanville, Hinkley Point C) show no clear twin-unit effect in public data, with FOAK and regulatory churn dominating. The 8% default lies below the midpoint of the 5–15% empirical range.

This factor is deliberately *not* a Wright’s-Law learning curve. Wright-style cost reductions apply to fleet-cumulative manufactured production (typically requiring fleet sizes in the hundreds to thousands), and the empirical fission literature on cross-program deployment finds no positive cross-program learning, with some analyses identifying *negative* learning at the program level for US and French nuclear [31, 32, 6]. Cross-fleet learning, if introduced in future work, belongs at a separate parameter representing cumulative units of a given concept built worldwide, not on n_{mod} , which represents units at a single site.

5.3.3 CAS22.01.03: Coils (Superconducting and Resistive)

CAS22.01.03 covers the magnet system: toroidal field (TF), central solenoid (CS), poloidal field (PF) coils, structural casing, insulation, quench protection, cryostat interfaces, and testing.

Conductor Scaling Law The conductor quantity in kA-m follows from the magnet topology. For a toroidal system the on-axis field fixes the total ampere-turns through Ampère’s law, $NI = 2\pi R_0 B / \mu_0$, while the conductor length per turn scales with the coil-bore radius r_{coil} (the winding encircles the plasma, blanket, shield, and vessel). The kA-m, and hence the cost, are therefore *bilinear* in the major radius R_0 and the coil bore r_{coil} :

$$C_{220103} = \frac{G \cdot B \cdot R_0 \cdot r_{\text{coil}}}{\mu_0 \times 1000} \times c_{\text{kAm}} \times M_{\text{concept}} \quad (\text{toroidal}). \quad (42)$$

For a linear device (mirror, FRC, dipole, pulsed) the magnet is a true circular loop or solenoid, for which $B = \mu_0 NI / (2R)$ and the turn length is $2\pi R$, giving the standard r^2 scaling $C_{220103} \propto G \cdot B \cdot r_{\text{coil}}^2 / \mu_0$. Here G is a geometry factor (tokamak: $4\pi^2$; stellarator: $4\pi^2 \times f_{\text{path}}$, the $f_{\text{path}} = 2$ capturing the roughly doubled length of a non-planar 3D winding; mirror: $n_{\text{coils}} \cdot 4\pi$, the sum over independent solenoids), B is the field at the loop centre / on axis (not the peak field on the conductor, which is a factor of about 2–4 higher for high-field superconductor but does not enter the ampere-metre quantity), c_{kAm} is the conductor cost per kA-metre, and M_{concept} is a manufacturing markup capturing winding, insulation, quench protection, structural casing, cryostat, and testing. Mirror coils are divided into two classes: $n_{\text{central}} = L/d_{\text{coil}}$ central-cell solenoids (continuous, spacing $d_{\text{coil}} = 5$ m by default) carrying ampere-metres at the coil design field b_{center} , plus $n_{\text{plug}} = 4$ high-field end-plug coils at the throat field $R_m B_{\text{min}}$, where R_m is the mirror ratio (throat field over midplane field) and B_{min} is the plasma midplane field (b_{center} and B_{min} are independent inputs). The geometry factor $G = (n_{\text{central}} + n_{\text{plug}}) \cdot 4\pi$ accumulates over all independent solenoids.

The coil-bore radius r_{coil} is taken as the outer radius of the vacuum vessel from the device’s radial build, since in a magnetic-confinement reactor the superconducting magnets sit outboard of the entire plasma–blanket–shield–vessel stack. The ARC point design places its TF coils beyond a 0.85 m inboard blanket/shield standoff [33], and ARIES-CS requires 1.5–2 m (1.79 m for a regular breeding module) between the plasma and the middle of the coil winding pack [34]. Deriving r_{coil} from the radial build, rather than treating it as a free parameter, ties the magnet cost to the same geometry that sets the blanket and shield volumes.

The two coil classes also carry different bores. The central solenoids enclose the full radial build, so their bore is the vessel outer radius plus an assembly standoff, $r_{\text{coil}} = r_{\text{vessel,out}} + 0.10$ m; the end-plug coils sit at the throat, where the plasma necks down by flux conservation and no breeding blanket extends, so their bore is the throat plasma radius (the midplane radius a reduced by $\sqrt{R_m}$) plus a throat standoff, $r_{\text{coil}} = a/\sqrt{R_m} + 0.30$ m. This small-bore high-field plug versus large-bore lower-field central split is the cost-relevant distinction unique to the mirror.

Table 9: CAS22.01.03 manufacturing markups and path factors by confinement concept.

Concept	Markup	Path factor	Ref. coil cost	Rationale
Tokamak	$3.09\times$	1.0	\$516M	TF+CS+PF complexity; calibrated at the SPARC-class reference ($B = 12$ T, $R_0 = 3.0$ m, $r_{\text{coil}} = 2.95$ m)
Stellarator	$5.87\times$	2.0	\$2,130M	Non-planar 3D coils; $1.9\times$ the tokamak markup, the NCSX modular-coil production cost overrun [35]
Mirror	$1.7266\times$	1.0	\$513M	Two-class: $n_{\text{central}} = L/d_{\text{coil}}$ central solenoids at b_{center} with bore $r_{\text{coil}} = r_{\text{vessel,out}} + 0.10$ m plus $n_{\text{plug}} = 4$ plug coils at the throat field $R_m B_{\text{min}}$ with bore $r_{\text{coil}} = a/\sqrt{R_m} + 0.30$ m; calibrated at the default 20 m chamber length
Pulsed FRC	$1.5\times$	1.0	n/a	Theta-pinch formation coils
Theta pinch	$1.5\times$	1.0	n/a	Compression coils
Orbitron	$1.5\times$	1.0	n/a	Electrostatic confinement
Polywell	$2.0\times$	1.0	n/a	Polyhedral magrid
Dipole	$3.0\times$	1.0	n/a	Floating coil + lift coils (see text)
MIF, IFE, Z-pinch	\$0 (no plant-scale confinement magnets)			Seed coils opt-in

Conductor Cost Assumptions The default conductor is REBCO high-temperature superconductor at \$50/kA-m, an aggressive NOAK target. Current market prices for REBCO tape are \$150–300/kA-m; the \$50/kA-m assumption reflects projected cost reductions from scaled-up manufacturing (analogous to the solar PV learning curve). For comparison, Nb₃Sn (the ITER conductor) is \$7/kA-m at maturity, and NbTi (LHC heritage) is similar.

This is a deliberate design choice: the model targets NOAK economics for a mature fusion industry, not FOAK procurement costs. For FOAK sensitivity analysis, the conductor cost may be overridden to \$150–300/kA-m, which roughly triples the coil account. Unlike B-11 enrichment (where the FOAK/NOAK gap reflects a missing industrial supply chain requiring \$10,000/kg falling to \$75/kg), the REBCO cost trajectory is a manufacturing learning curve for an existing product, making the aggressive target more defensible.

Resistive Copper Coils The \$/kA-m model is correct where an expensive superconductor dominates cost. For low-field resistive copper coils (an FRC at near-unity beta runs external fields of order 0.1–1 T) the conductor is cheap per kA-m, so that basis yields a near-zero, unphysical figure while the machine still requires tonnes of copper to wind and support. When the conductor material is copper, the account is instead a *mass build-up* that re-prices the same ampere-metres by mass:

$$C_{220103} = \frac{1}{10^6} (m_{\text{Cu}} p_{\text{Cu}} k_{\text{Cu}} + m_{\text{st}} p_{\text{st}} k_{\text{st}}), \quad (43)$$

with $m_{\text{Cu}} = (\rho_{\text{Cu}}/J)$ (ampere-metres), $\rho_{\text{Cu}} = 8960$ kg/m³, current density $J = 5$ A/mm², copper price $p_{\text{Cu}} = 11$ \$/kg, fabrication markup $k_{\text{Cu}} = 3.5$, steel support mass $m_{\text{st}} = 0.6 m_{\text{Cu}}$, $p_{\text{st}} = 6$ \$/kg, and $k_{\text{st}} = 3.0$. The ampere-metres are the same $G B r_{\text{coil}}^2/\mu_0$ quantity as the superconducting path, so no new geometry assumption is introduced. This mass build-up is used whenever the conductor material is copper, so it applies to every copper concept (steady and pulsed FRC, theta pinch, polywell, orbitron) and leaves superconducting concepts on the \$/kA-m path. A steady FRC at $B = 0.5$ T, $R = 1.85$ m, $n_{\text{coils}} = 4$ carries about 123 t of copper and 74 t of steel, giving $C_{220103} \approx$ \$6M, versus about \$0.1M from the \$/kA-m path at the same field.

Levitated Dipole Floating Coil The levitated dipole replaces the external magnet set with a single superconducting floating coil immersed in the plasma, so its CAS22.01.03 follows a dedicated build-up rather than eq. (42). The floating coil's conductor quantity is the single-ring value $4\pi B_{\text{center}} R_{\text{coil}}^2 / \mu_0$ (geometry factor $G = 4\pi$ as for one mirror solenoid), priced on the same \$/kA-m conductor basis but carrying a higher markup ($M_{\text{lev}} = 8$) for the float, no-access engineering: a persistent-current joint, an integral cryostat, and inductive charging with no demountable leads. The external stationary lift coils that hold the floating coil against gravity are taken as a fixed fraction (default 0.10) of the floating-coil cost, and an integral cryostat term covering neon-slush cooling, the flux pump, and levitation control is added as a flat \$100M:

$$C_{220103} = M_{\text{lev}} c_{\text{float}} + f_{\text{lift}} M_{\text{lev}} c_{\text{float}} + c_{\text{cryo}}, \quad (44)$$

with $f_{\text{lift}} = 0.10$ and $c_{\text{cryo}} = 100$ M\$. The reference OpenStar Reactor A point uses $B_{\text{center}} = 6.26$ T and $R_{\text{coil}} = 5.3$ m.

5.3.4 CAS22.01.04: Supplementary Heating / Primary Driver

CAS22.01.04 covers different hardware depending on the confinement family.

Steady-State MFE For tokamaks, stellarators, and mirrors, the account covers vendor-purchased auxiliary heating systems. Cost scales linearly with installed power:

$$C_{220104} = \sum_i c_i P_i \quad [\text{M\$}] \quad (45)$$

where $c_{\text{NBI}} = 7.46$, $c_{\text{ICRF}} = 4.38$, $c_{\text{ECRH}} = 5.28$, $c_{\text{LHCD}} = 4.23$ (all M\$/MW). The per-MW costs are calibrated to ITER procurement contracts, adjusted from FOAK to NOAK.

The split P_i is priced per MW of *injected* heating power, the same P_{in} the power balance uses ($q_{\text{sci}} = P_{\text{fus}}/P_{\text{in}}$); the wall-plug draw $P_{\text{in}}/\eta_{\text{pin}}$ enters the recirculating power, not this capital line. To keep the costed power identical to the power-balance power, the split is the heating *mix* and is normalized so $\sum_i P_i = P_{\text{in}}$; overriding P_{in} rescales the split, so the costed heating remains consistent with the power balance. A fully zero split (electrostatic concepts whose input power is not NBI/RF heating, e.g. orbitron, polywell) stays zero, leaving their heating capital at \$0. Pricing the supply-dominated NBI capital on wall-plug power $P_{\text{in}}/\eta_{\text{pin}}$, which would auto-elevate low-coupling concepts such as the FRC, is a deliberate refinement not applied here; the driver's recirculating burden is already represented through η_{pin} .

Pulsed Concepts For pulsed concepts, the account covers the primary driver capital, namely the hardware that compresses or ignites the target. This is the pulsed analog of the magnet system (CAS22.01.03): the mechanism that provides confinement. The cost basis depends on the driver type.

Lasers, accelerators, and electromagnetic guns are costed per joule of pulse energy. Their capital is set by the per-pulse energy (laser aperture, amplifier and pump-diode count, accelerator beam energy and storage-ring charge, coaxial-gun size and peak current) and not by how often the driver fires. Repetition rate adds cooling and consumable replacement, which are sub-dominant capital and operating costs rather than a multiplier on the driver hardware itself. Costing on average power $E_{\text{drv}} f_{\text{rep}}$ would instead price one physical laser, across the 0.1 to 15 Hz range of concept repetition rates, as if it were a hundred distinct machines. Hence

$$C_{220104} = c_{\text{drv}}^E \times E_{\text{drv}} \quad [\text{M\$}] \quad (46)$$

with c_{drv}^E in M\$/MJ. Pneumatic and mechanical injectors (mag-target) instead accelerate target mass on every shot, so throughput (average power) drives their hardware count, handling, and recirculation plant, and they retain an average-power basis with $P_{\text{drv}} = E_{\text{drv}} f_{\text{rep}}$:

$$C_{220104} = c_{\text{drv}}^P \times P_{\text{drv}} \quad [\text{M\$}] \quad (47)$$

These coefficients are NOAK projections; table 10 lists them. The heavy-ion figure evaluates the underlying \$/W estimate at its reference repetition rate (\$12/W at 5 Hz gives 60 M\$/MJ) and then holds constant. The laser figure takes the published diode-pumped solid-state (DPSSL) NOAK range of \$210–700/J at its aggressive end: the optics and diode array cost \$205/J here, with the small (\$5/J) capacitor bank that fires the diodes costed in CAS22.01.07, for a \$210/J turnkey driver. It branches on `laser_driver_type` (DPSSL default at 205, KrF excimer at 40 with engineering range 20–200, and flashlamp Nd:glass NIF-class at 1000 M\$/MJ); the electromagnetic guns follow the same per-pulse logic.

Driver scheduled replacement. A rep-rated laser driver's replaceable subsystems wear at shot lifetimes spanning sub-annual to multi-decade, so each is charged as the level annual cost of replacing it every $t = N_{\text{life}}/\dot{N}_{\text{shot}}$ years over the plant life, summed by the same geometric replacement model used for the core, direct-energy-converter grid, and

Table 10: CAS22.01.04 driver cost coefficients by pulsed concept.

Concept	Basis	Coeff.	Hardware
Laser IFE	M\$/MJ	205	Diode-pumped solid-state laser
Heavy ion	M\$/MJ	60	RF linac + storage rings
Plasma jet	M\$/MJ	4	Plasma gun array
Staged Z-pinch	M\$/MJ	1.5	Coaxial gun + gas injection
MagLIF	M\$/MJ	205	Laser preheat (DPSSL); main driver in CAS22.01.07
Mag. target	M\$/MW	3	Pneumatic pistons, liquid metal loop
Z-pinch, DPF	n/a	0	Driver is electrical (CAS22.01.07)
Pulsed FRC, Theta pinch	n/a	0	Driver is coils (CAS22.01.03)

capacitor bank. The first set is capital (already in CAS22.01.04); only replacements beyond it are charged. For DPSSL the pump diodes carry a NOAK shot life (about 10^{10}) that exceeds a 30-year plant at 10 Hz, so they are effectively a capital item and the operating burden is dominated by the final optics; for flashlamp-pumped Nd:glass the lamp shot life (about 10^4) is sub-annual and the replacement term is prohibitive, the established reason NIF-class drivers are not viable for rep-rated energy.

For MagLIF the main driver is the electrical Z-pinch, costed in CAS22.01.07; the only CAS22.01.04 contribution is an optional laser preheat, costed per joule of preheat pulse energy $c_{\text{pre}} E_{\text{pre}}$ on the same diode-pumped solid-state laser basis as the IFE driver. Magnetized-compression concepts that omit the preheat laser set $E_{\text{pre}} = 0$ and incur no preheat cost, while the coefficient remains available for those that include one.

Concepts whose driver is purely electrical (pulsed power / capacitor bank) have their driver capital captured entirely in CAS22.01.07 on a \$/J stored basis, avoiding double-counting. Similarly, concepts whose confinement is provided by coils (pulsed FRC, theta pinch) have that hardware in CAS22.01.03.

5.3.5 CAS22.01.06: Vacuum System

CAS22.01.06 is a sum of two parts with different cost drivers:

$$C_{220106} = C_{\text{vessel}} + C_{\text{pump}}. \quad (48)$$

The *vessel shell* (welded stainless chamber, ports, gauges, leak detection) is volume-based, scaling with reactor size:

$$C_{\text{vessel}} = c_{\text{ves}} V_{\text{ves}} \left(\frac{P_{\text{et}}}{P_{\text{et,ref}}} \right)^{0.6}, \quad c_{\text{ves}} = 0.72 \text{ M}\$/\text{m}^3, \quad (49)$$

where $P_{\text{et,ref}} = 1100 \text{ MWe}$ is the reference gross electric power (net plus recirculating, for a 1 GWe-net reference plant); it is the common gross-electric normalization for the buildings (CAS21), structure, power-supply (eq. (53)), and remote-handling accounts. The *pumping* system is sized by gas throughput, not vessel volume. A pump of speed S removes a throughput $Q = SP$, so the installed speed required to hold an operating (plenum) pressure P_{op} is $S_{\text{req}} = Q_{\text{gas}}/P_{\text{op}}$, costed at $c_{\text{pump}} = 0.015 \text{ M}\$$ per (m^3/s) (commodity cryopump procurement, $\$15/(\text{L}/\text{s})$). The gas load has two sources; wall outgassing scales with surface area but is negligible for a baked UHV system and is omitted:

$$Q_{\text{NBI}} = g \frac{P_{\text{NBI}}}{E_b} k_B T, \quad (50)$$

$$Q_{\text{fuel}} = n_{\text{ion}} \frac{1 - f_b}{f_b} \frac{P_{\text{fus}}}{E_{\text{fus}}} k_B T, \quad (51)$$

with $T = 300 \text{ K}$, gas amplification $g = 1$ (gas particles pumped per beam particle, calibrated to the C-2W machine's roughly $2000 \text{ m}^3/\text{s}$ divertor pumping), reference NBI energy $E_b = 120 \text{ keV}$ (the NBI gas load scales as $1/E_b$), $n_{\text{ion}} = 2$ ions consumed per reaction, and E_{fus} the fuel-dependent energy per reaction. The pumping cost is then

$$C_{\text{pump}} = c_{\text{pump}} \frac{Q_{\text{NBI}} + Q_{\text{fuel}}}{P_{\text{op}}}. \quad (52)$$

The operating pressure P_{op} is the dominant, concept-specific driver, set per concept: a few Pa for tokamak and stellarator divertor plenums (high-recycling regions designed to pump at high pressure), versus 0.02–0.05 Pa for open-field-line linear devices (mirror, FRC) that must hold a low neutral pressure to limit charge-exchange losses. The same throughput

therefore costs an FRC roughly $60\times$ more to pump than a tokamak. The fueling term dominates over the NBI term at reactor beam energies; because aneutronic $p\text{-B}^{11}$ releases about half the energy per reaction of D-T, it runs about twice the reaction rate and pumps about twice the fuel throughput at equal fusion power. The pumping model applies uniformly to every concept, so these differences follow from the inputs rather than per-concept manual adjustment.

Reporting convention. Where a single account aggregates components with distinct cost bases, the model emits informational sub-lines keyed $\langle \text{CODE} \rangle_{\langle \text{component} \rangle}$ (here C220106_vessel and C220106_pump) alongside the canonical total. These sub-lines are excluded from all aggregation and exist only for visibility and sensitivity tracing. CAS22.01.06 is currently the sole account that uses them.

5.3.6 CAS22.01.07: Power Supplies / Pulsed Driver Store

CAS22.01.07 covers the electrical power supply systems that drive the fusion core: magnet power supplies, pulsed power drivers, and associated switchgear. The account has two modes.

Steady-State MFE For tokamaks, stellarators, and mirrors, the cost scales with gross electric output:

$$C_{220107} = c_{ps} \times (P_{et}/P_{et,ref})^{0.7} \quad [\text{M\$}] \quad (53)$$

where $c_{ps} = \$80\text{M}$ is the power-supply reference cost at $P_{et,ref}$ (section 5.3.5). It originates from the ARIES-CS design study (\$70.6M in 2004\$ for a 1.3 GWe stellarator, approximately \$78/kW). Cross-checks against GW-scale HVDC converter stations (\$100–250/kW installed)² and utility-scale solar inverters (\$30–50/kW [30]) bound the reference value: fusion magnet supplies operate at lower voltage and higher current than HVDC, the lower-cost regime for power electronics. No direct vendor quote exists at fusion-relevant parameters (1–10 kV, 10–100 kA, 100+ MW). Uncertainty: $\pm 20\%$.

Pulsed Concepts For all pulsed concepts, the cost scales with stored energy per pulse on a \$/J basis:

$$C_{220107} = c_{cap} \times E_{stored} \quad [\text{M\$}] \quad (54)$$

where $c_{cap} = 0.50 \text{ \$/J}$ is the NOAK all-in installed cost (capacitors, switches, charging supplies, buswork). This is an aggressive target: present lab-scale pricing is \$20–50/J, a $40\text{--}100\times$ gap. The CATF IWG extension [5] recommends \$1.5–4/J for NOAK. The \$0.50/J default assumes advanced-dielectric capacitors manufactured at high volume, a commercial viability requirement, not a current capability.

Capacitor banks require scheduled replacement (CAS72). At $f_{rep} = 1 \text{ Hz}$ and 85% availability, the bank executes 27 million cycles per year. At the NOAK baseline lifetime of 10^8 shots, replacement occurs every 3.7 years. The annualized replacement cost is computed as a present-value sum of discrete replacements over the plant lifetime, discounted at the project interest rate.

5.3.7 CAS22.01.08: Divertor / Target Factory

Divertor The divertor sub-account (CAS22.01.08) keeps the inherited pyFECONS scaling for steady-state MFE concepts that exhaust onto a material target,

$$C_{220108} = c_{div} (P_{th}/1000)^{0.5}, \quad (55)$$

with $c_{div} = 60 \text{ M\$}$ the reference cost at 1 GWth (the 1000 normalizes the thermal power P_{th} to GW). Concepts that exhaust charged particles without a material target carry no manufactured divertor cassette and $C_{220108} = 0$: the levitated dipole (closed-field-line topology, loss-cone exhaust at the chamber openings) and the electrostatic concepts (orbitron, polywell), which direct charged particles to the direct energy converter.

Target Factory For inertial and magneto-inertial concepts the same sub-account funds the on-site target factory, a per-concept bottom-up build-up over three drivers,

$$C_{220108} = c_{fix} + c_{line} f_{rep} + c_{flow} (P_{fus}/1000) : \quad (56)$$

a fixed building and tritium-confinement shell (c_{fix}); precision production lines that scale with throughput, i.e. the repetition rate f_{rep} (c_{line}); and material handling, cryogenics, and post-shot recovery that scale with mass-energy flow P_{fus} normalized to 1 GW of fusion power (c_{flow}). A separate target-size term is unnecessary: at fixed module count the per-shot yield P_{fus}/f_{rep} is determined by these two variables, and target size follows from the yield.

²HVDC converter station vendor literature, Siemens Energy and Hitachi ABB Power Grids, 2022–2024.

The two factory archetypes differ substantially in cost. A laser or heavy-ion capsule factory is a precision cleanroom whose tritium-handling back half (DT fill, ice-layering, contained assembly, injection) adds a dual-confinement premium and whose throughput is oversized by the inverse acceptance yield; it totals about 725–780 M\$, calibrated so its optimistic corner reproduces the LIFE [36] target factory (about \$600 M, \$0.25/target). A MagLIF or Z-pinch load is instead a stamped-and-filled metal liner, a casting-shop process near 150 M\$, roughly a factor of five lower in cost.

The per-shot target cost (section 5.13) is sourced from fully-loaded studies that already amortize the plant, so the capital and per-shot accounts are kept disentangled to count the factory once. A factory is carried only when the per-shot target cost $c_{\text{target}} > 0$, and is sized by c_{fac} ; concepts that form their plasma or liner in situ (plasma-jet MIF, the liquid-liner magnetized-target loop, pulsed FRC, theta pinch, dense plasma focus, and sheared-flow / staged Z-pinch) set both to zero and carry $C_{220108} = 0$.

5.3.8 CAS22.01.09: Direct Energy Converter (venetian blind)

CAS22.01.09 covers add-on direct energy converters for linear devices (mirrors and steady-state FRCs) where charged-particle exhaust escapes along open field lines and can be decelerated to recover kinetic energy as electricity. Inductive DEC for pulsed-FRC architectures is captured in CAS22.01.07 via Q_{sci} -derived markups on the driver bank (section 5.3.6); the present subsection covers the electrostatic venetian-blind variant for steady-state mirrors.

The cost scales with DEC electric output:

$$C_{220109} = c_{\text{dec}} \times (P_{\text{dec}}/P_{\text{dec,ref}})^{0.7} \quad [\text{M\$}] \quad (57)$$

where $c_{\text{dec}} = 125$ M\$ is the NOAK all-in reference cost at $P_{\text{dec,ref}} = 400$ MWe DEC electric output, and the 0.7 exponent reflects sub-linear scaling of vacuum/tank infrastructure with throughput while grid modules and power conditioning scale roughly linearly.

The reference figure is a bottom-up build-up of the DEC-specific add-on hardware, excluding shared mirror infrastructure already costed under CAS22.01.06 and the expander. Table 11 lists the component costs and their procurement anchors. The central hardware subtotal is \$109 M; adding 15% NOAK installation gives the \$125 M used for c_{dec} . Uncertainty is $\pm 35\%$, dominated by the HV power-conditioning scale-up factor and the plant-scale tank fabrication unit cost.

Table 11: Venetian-blind DEC add-on hardware build-up (M\$). The central total, plus 15% NOAK installation, sets c_{dec} .

Component	Range	Central	Basis
Tank	3–15	7	Fabricated 304L vacuum shell (10–15 m \times 20–40 m), refinery-hydrocracker class [37], vacuum-only collapse load
HV power conditioning	35–55	45	IGBT/DC-conversion chain at 60–70% of VSC HVDC valve-hall cost [38]
Cryopumps	10–25	15	10^6 – 10^7 L/s; ITER procurement [39] and industrial pricing
Heat collection panels	10–20	15	Hypervapotron W panels for the 30–90 MW load, ITER NBI ion-dump analog [40]
Grid & collector modules	10–20	15	W ribbon grids, Hoffman [41] area cost; TMX cross-check [42]
Misc	10–17	12	HV bushings, vacuum gate valve, controls, instrumentation
Hardware subtotal	78–152	109	

5.3.9 CAS22.01.10: Remote Handling & Maintenance Equipment

CAS22.01.10 covers the robotic and remotely-operated equipment required for in-vessel maintenance: manipulators, transfer casks, in-pipe welding/cutting tools, and rad-hardened actuators. The building that houses this equipment (hot cell) is costed separately in CAS21.

The cost model is:

$$C_{220110} = C_{\text{RH,base}}(f) \times S_{\text{concept}} \times \left(\frac{P_{\text{et}}}{P_{\text{et,ref}}} \right)^{0.5} \quad (58)$$

where $C_{\text{RH,base}}(f)$ is a fuel-dependent base cost (M\$ at 1 GWe tokamak reference) and S_{concept} is a geometry-dependent scaling factor.

Fuel Dependence Neutron activation determines whether remote handling is needed and how heavily equipment must be rad-hardened. Table 12 lists the base costs.

Table 12: Remote handling base costs by fuel cycle (1 GWe tokamak reference).

Fuel	Base (M\$)	Rationale
D-T	150	Full RH suite, rad-hardened to 14.1 MeV neutrons
D-D	100	Same scope, reduced rad-hardening (2.45 MeV)
D- ³ He	30	Lighter duty, activation still exceeds occupational limits
p- ¹¹ B	20	Conventional maintenance equipment (no rad-hardening)

Concept Dependence Toroidal vessels (tokamak, stellarator) require articulated multi-axis manipulators to reach components through narrow ports, while open and end-access geometries (mirror, FRC, and the other non-toroidal concepts) permit simpler tooling. Toroidal concepts use $S_{\text{concept}} = 1.0$; all non-toroidal concepts use $S_{\text{concept}} = 0.55$.

5.3.10 CAS22.01.12: Isotope Separation

CAS22.01.12 is set to zero for all fuel cycles: isotope procurement is modeled as market purchase in CAS80 at enriched unit prices. On-site separation-plant capital (CAS22.01.12) and enriched market prices (CAS80) are mutually exclusive models of the same cost, so charging both would double-count separation. Market purchase is adopted because on-site separation is not justified at fusion-scale consumption rates. Tritium is the exception: it is bred on-site in the blanket and processed by the fuel handling system (CAS22.05), not purchased.

5.3.11 CAS22.02–.07: Plant-Wide Reactor Systems

The remaining CAS22 sub-accounts are inherited with pyFECONS scaling rather than re-derived: each cost term is a reference cost scaled by a plant-power ratio,

$$C = c_{\text{ref}} (P/P_{\text{ref}})^{\alpha}, \quad (59)$$

with the reference cost c_{ref} , normalized power P/P_{ref} , and exponent α in table 13; these are pyFECONS reference-plant values, inherited pending re-derivation.

Table 13: Inherited plant-wide reactor systems (CAS22.02–.07): reference cost c_{ref} , normalized power P/P_{ref} (P_{ref} in MW), and exponent α per cost term (eq. (59)). The CAS22.05 reference cost is fuel-dependent (listed D-T/D-D/D-³He/p-¹¹B); the others are fuel-agnostic.

Account	Sub-system	c_{ref} (M\$)	P/P_{ref}	α
CAS22.02	Primary coolant	166	$P_{\text{net}}/1000$	1.0
	Intermediate coolant	40.6	$P_{\text{th}}/3500$	0.55
CAS22.03	Auxiliary coolant	1.10	$P_{\text{th}}/1000$	1.0
	Cryoplant	200	$P_{\text{cryo}}/30$	0.7
CAS22.04	Radioactive waste management	1.96	$P_{\text{th}}/1000$	1.0
CAS22.05	Fuel handling & storage	120/60/40/15	$P_{\text{net}}/1000$	0.7
CAS22.06	Other reactor plant equipment	11.5	$P_{\text{net}}/1000$	0.8
CAS22.07	Instrumentation, control, diagnostics	85	$P_{\text{th}}/3500$	0.65

5.4 CAS23–26: Balance of Plant Equipment

CAS23–26 cover conventional power-conversion and electrical infrastructure. These accounts are **fuel-independent**: the choice of fuel affects the reactor island (CAS22) but not the turbine hall, switchyard, or cooling towers.

The model supports three thermal cycles, selected by the user: steam Rankine, supercritical CO₂ (sCO₂) Brayton, and combined cycle (gas topping plus steam bottoming). The cycle determines the thermal conversion efficiency η_{th} and the per-MW coefficients for CAS23 (turbine plant) and CAS26 (heat rejection). CAS24 (electrical equipment) and CAS25 (miscellaneous plant) are cycle-independent.

CAS23 (turbine plant) scales with thermal electric power $P_{\text{the}} = \eta_{\text{th}} P_{\text{th}}$, and CAS26 (heat rejection) scales with total thermal power P_{th} . This ensures both accounts auto-zero for pure direct energy conversion plants ($\eta_{\text{th}} = 0$) and scale

correctly for hybrid DEC-plus-thermal configurations. CAS24 and CAS25 scale with gross electric P_{et} :

$$C_{23} = n_{\text{mod}} P_{\text{th}} c_{23}, \quad C_{26} = n_{\text{mod}} P_{\text{th}} c_{26}, \quad C_{24,25} = n_{\text{mod}} P_{\text{et}} c_{2x} \quad (60)$$

where c_{2x} is a per-MW coefficient (M\$/MW). Table 14 lists the adopted values for each cycle.

Table 14: Balance of plant per-MW coefficients by thermal cycle.

CAS	Scope	Rankine	sCO ₂	Combined
23	Turbine plant equipment	0.203	0.159	0.241
24	Switchyard, transformers, cabling	0.086	0.086	0.086
25	Fire protection, compressed air, HVAC	0.053	0.053	0.053
26	Cooling towers, circulating water	0.035	0.023	0.018
η_{th}		0.40	0.47	0.53

The Rankine coefficients derive from the ARIES cost-account tradition [43], calibrated against the NETL *Cost and Performance Baseline for Fossil Energy Plants* [29].

The sCO₂ Brayton efficiency of $\eta_{\text{th}} = 0.47$ reflects the DOE/Sandia target of 45–50% for recompression Brayton cycles at nuclear heat source temperatures (500–700°C) [44, 45]. The CAS23 coefficient is 22% below Rankine: sCO₂ turbomachinery is 85% smaller by volume, but recuperators add cost, netting 20% overall reduction [46].

The combined cycle efficiency of $\eta_{\text{th}} = 0.53$ is derived from NGCC performance (>60%, National Energy Technology Laboratory 29), adjusted downward for fusion heat source temperatures (600°C vs. 1500°C gas turbine inlet). The CAS23 coefficient is 19% above Rankine due to dual turbomachinery sets (topping plus bottoming) and a heat recovery steam generator (HRSG).

The adopted Rankine coefficients are consistent with the NREL ATB 2024 nuclear cost breakdown [30], which allocates 3.9% of total capital to energy conversion and 6.3% to electrical equipment: the adopted fractions fall at or below these, as expected for the conventional, non-nuclear-grade balance of plant assumed at NOAK.

5.5 CAS27: Special Materials

CAS27 covers the initial inventory of non-fuel reactor materials: breeding blanket fill, neutron multiplier, and other special inventory. CAS22.01.01 covers the blanket *structure*; CAS27 covers the *material that fills it*. A material inventory is set by blanket volume, not net electric power, so CAS27 is a volume-based mass build-up keyed on the blanket fill:

$$C_{27} = V_{\text{blk}} \cdot \nu(\text{fill}) \cdot \rho(\text{fill}) \cdot c(\text{fill}) \quad (61)$$

where V_{blk} is the blanket volume of eq. (40) (first-wall, blanket, and reflector), ν the fraction of that region occupied by the costed material (liquid fill fraction; or breeder/multiplier-zone \times pebble packing ≈ 0.25 for solid pebble beds), ρ its density, and c its unit price.

The blanket configuration is specified as an orthogonal pair: a `BlanketForm` (structural architecture, driving $s(\text{form})$ in CAS22.01.01) and a `BlanketFill` (bulk material, driving the inventory here). Compatibility between form and fill is enforced at validation time. Fuel-appropriateness enters through the chosen fill: aneutronic / non-breeding concepts use `none` and recover zero. Table 15 lists the per-fill inputs.

Table 15: CAS27 blanket-fill inventory inputs (volume-based build-up).

Fill	ρ (kg/m ³)	ν	c (\$/kg)	Basis
pbli	9400	0.50	5	Pb-17Li (99.3% Pb) + enriched Li-6 premium
li	490	0.80	200	liquid Li, Li-6 enrichment (\$80–1000/kg)
flibe	1940	0.80	150	2LiF-BeF ₂ , Be-dominated (NOAK)
be_ceramic	1850	0.25	700	HCPB Be multiplier; Li-ceramic folded in
ceramic_only	2400	0.25	150	Li-ceramic breeder pebbles
li2o	2013	0.25	150	Li ₂ O ceramic
none	–	–	–	Aneutronic, no breeder

Scaling by the modelled blanket volume rather than a power-law keeps CAS27 consistent with the blanket structure (CAS22.01.01) and the other volume-based reactor-component accounts, and it costs both a compact high-power-density

design (e.g. an ARC-class FLiBe immersion blanket, about \$100M) and a large thin-shell design (e.g. a levitated dipole's Li₂O blanket) by their actual material volume.

The HCPB (be_ceramic) inventory is dominated by global beryllium supply: world production is 300 tonnes/yr, so a single DEMO-scale plant consumes the entire annual supply, making the beryllium cost the largest known discriminator in the EUROfusion blanket selection process.

Aneutronic fuels (D-He3, p-B11) typically use none/none (no breeding blanket), recovering minimal special-material inventory.

5.6 CAS28: Digital Twin

CAS28 covers a plant-wide operations digital twin for operator training, predictive maintenance, and operational optimization; it is not a plasma physics or real-time plasma-control model. Plasma control and diagnostics are costed under instrumentation and control (CAS22.07, table 13). A fixed cost of \$5M is adopted, independent of plant size, fuel type, or number of modules: the digital twin is software-dominated, and its complexity scales with the number of modeled subsystems rather than plant capacity.

The \$5M figure is anchored to disclosed advanced-reactor digital-twin budgets. Under the DOE ARPA-E GEMINA program [47], the University of Michigan received \$5.2M to develop a scalable reactor digital twin (first validated on a campus molten-salt loop, then applied to the Kairos Power design), alongside a complementary \$2.2M Argonne award for O&M automation. A single plant-wide reactor twin therefore corresponds to the adopted \$5M, consistent with industrial digital twin deployments for large thermal plants (\$2–10M; Siemens MindSphere, GE Predix, AVEVA).

5.7 CAS29: Contingency on Reactor Plant Equipment

CAS29 applies the contingency rate f_{cont} (defined above) to the sum of the CAS20-series reactor-plant-equipment accounts CAS21–28:

$$C_{29} = f_{\text{cont}} \times \sum_{i=21}^{28} C_i. \quad (62)$$

5.8 CAS30: Capitalized Indirect Service Costs

CAS30 covers construction support services not attributable to specific plant systems: field indirect costs (equipment rental, temporary structures, consumables), construction supervision, and offsite design services [3].

An aggregate model is adopted:

$$\text{CAS30} = f_{\text{indirect}} \times \text{CAS20} \times \frac{T_c}{T_{\text{ref}}} \quad (63)$$

where $f_{\text{indirect}} = 0.20$ (default), T_c is the construction time, and $T_{\text{ref}} = 6$ yr is a reference duration. The construction-time scaling captures the primary driver that varies between scenarios.

No fusion construction data exists at this granularity to calibrate CAS30, so the 20% default is set by triangulation against established conventions: below Schulte's 35% of total direct cost [1] (a 1978 fission baseline, high for NOAK fusion); below the Miller/ARIES value of 23.2% [2, 48, 49]; above the labor-only pyFECONS staffing figure of 5.8% [4]; and consistent with efficient NOAK nuclear construction internationally (15–20% of total direct cost). Sub-account precision (CAS31/CAS32/CAS35 splits) is not empirically distinguishable for fusion and is not modeled.

5.9 CAS40: Capitalized Owner's Costs

CAS40 covers one-time costs incurred by the plant owner during construction to build an operating organization before commercial operation: staff recruitment and training (CAS41), staff housing/relocation (CAS42), and salary-related costs during the pre-operational period (CAS43) [3, 50].

CAS40 shares the same fuel-specific staff pool as CAS70 (section 5.12) but covers the pre-COD period rather than annual operation, so there is no double-counting. It scales with plant-total net electric power as

$$\text{CAS40} = C_{\text{owner}}(f) \times \left(\frac{P_{\text{net}} n_{\text{mod}}}{P_{\text{ref}}} \right)^{0.5} \quad (64)$$

where $C_{\text{owner}}(f)$ is a fuel-dependent base cost (M\$ at 1 GWe reference) and the 0.5 exponent, shared with CAS70, follows from staff-count scaling in the S-PRISM/INL data [50]. The base costs (table 16) apply the INL first-principles staffing build-up (training overhire, relocation, and pre-operational benefits, totalling roughly $3.2\times$ annual labor-plus-benefits) to the fuel-specific headcounts.

Table 16: Capitalized owner’s cost by fuel cycle (1 GWe reference).

Fuel	Staff	Base (M\$)	Key drivers
D-T	117	41.2	Tritium systems training, HP dept, radwaste, remote handling
D-D	94	32.8	Reduced neutron/tritium scope
D- ³ He	69	24.3	Light HP program, minor tritium
p- ¹¹ B	59	21.1	Near-industrial, radiation safety officer (RSO) only

The staffing basis yields 1–2% of total direct cost, well below the fission-level staffing that LSA-factor methods imply, reflecting the $4\text{--}8\times$ headcount reduction under Part 30 regulation.

5.10 CAS50: Capitalized Supplementary Costs

CAS50 covers capitalized items beyond direct construction, indirect services, and owner’s costs that must be incurred before commercial operation. CAS50 is decomposed into six sub-accounts, three of which are fuel-dependent:

$$\text{CAS50} = \underbrace{C_{51} + C_{53} + C_{54}}_{\text{fuel-independent}} + \underbrace{C_{52} + C_{55} + C_{56}}_{\text{fuel-dependent}} + C_{59} \quad (65)$$

where CAS20 is the direct capital account and CAS30 the capitalized indirect services. The sub-accounts are detailed below; the fuel-dependent parameters (s_{spare} , startup fuel, and the decommissioning provision) are collected in table 17.

5.10.1 CAS51: Shipping and Transportation

$$C_{51} = s_{\text{ship}} \text{CAS20}, \quad s_{\text{ship}} = 1.5\%. \quad (66)$$

The World Nuclear Association reports transportation at 2% of overnight cost for fission [51]; fusion avoids the extreme mass of reactor pressure vessels and containment structures, so a lower fraction is adopted.

5.10.2 CAS52: Spare Parts

$$C_{52} = s_{\text{spare}}(f) \sum_{i=22}^{28} C_i, \quad (67)$$

the initial on-site inventory at commercial operation, taken as a fuel-dependent fraction $s_{\text{spare}}(f)$ of reactor-plant and balance-of-plant capital. D-T plants require spare blanket modules, first-wall tiles, and divertor cassettes because of neutron damage, whereas p-¹¹B plants need only conventional industrial spares.

5.10.3 CAS53: Taxes

$$C_{53} = s_{\text{tax}} \text{CAS20}, \quad s_{\text{tax}} = 1\%. \quad (68)$$

Sales and use tax on construction materials, net of exemptions typical for large energy projects (for example NY RPTL §485 and state manufacturing-equipment exemptions).

5.10.4 CAS54: Construction Insurance

$$C_{54} = s_{\text{ins}} (\text{CAS20} + \text{CAS30}), \quad s_{\text{ins}} = 1.5\%. \quad (69)$$

Builder’s-risk premiums for large projects are typically 1–3% of insured value. Under Part 30, fusion avoids the Price-Anderson nuclear liability insurance required for Part 50 reactors.

5.10.5 CAS55: Startup Fuel and Inventory

$$C_{55} = c_{\text{fuel}}(f) \frac{P_{\text{net}} n_{\text{mod}}}{P_{\text{ref}}}, \quad (70)$$

the fusion analogue of the fission “first core” (3% of overnight cost, \$120M for a 1 GWe PWR). D-T requires 1–2 kg of tritium at \$30,000/g (\$40M); p-¹¹B requires only commodity hydrogen and boron (<\$0.1M).

5.10.6 CAS56: Decommissioning Provision

$$C_{56} = c_{\text{dec}}(f) \frac{P_{\text{net}} n_{\text{mod}}}{P_{\text{ref}}}, \quad (71)$$

the present value of the future decommissioning obligation. Fission decommissioning costs \$750–1,250/kWe (OECD-NEA median \$1,000/kWe) [52], driven by spent-fuel management, long-lived actinide disposal, and Part 50 regulatory overhead. Fusion avoids the spent-fuel and actinide burden (activated materials decay to clearance levels within 50–100 years [53]) and is regulated under the lighter Part 30, but dismantling the large activated structure (vessel, blanket, shield, magnets) with remote handling, together with D-T tritium decontamination, keeps the dismantling cost comparable to fission.

The D-T provision is therefore anchored at \$600/kWe: the fission reference less the spent-fuel (\$300/kWe) and actinide-disposal (\$200/kWe) drivers that fusion lacks, with near-fission dismantling and remote handling retained and D-T tritium decontamination added. Lower-activation fuels scale down accordingly. The capitalized provision is the present value of this obligation over a 40-year plant life at a 2% real discount rate (PV factor ≈ 0.45). The 2% rate is the conservative real return assumed for a segregated decommissioning trust fund (NRC 10 CFR 50.75 default earnings credit; OECD-NEA practice), not the plant's higher cost of capital, since such funds are escrowed in low-risk instruments.

5.10.7 CAS59: Contingency

$$C_{59} = f_{\text{cont}} \sum_{i=51}^{56} C_i, \quad (72)$$

the contingency on the CAS50 sub-accounts, applied at the same rate f_{cont} as the other direct accounts (section 5).

Table 17 summarizes the adopted values.

Table 17: CAS50 fuel-dependent parameters (1 GWe reference). The decommissioning row is the capitalized present value (PV factor 0.45) of the undiscounted end-of-life obligation (\$600/kWe for D-T).

Sub-account	D-T	D-D	D- ³ He	p- ¹¹ B
CAS52 spare parts (% of CAS22–28)	3%	2.5%	1.5%	1%
CAS55 startup fuel (M\$)	40	0.1	10	0.1
CAS56 decom. provision, PV (M\$)	272	199	140	113
<i>CAS50 total at 1 GWe (M\$)</i>	<i>638</i>	<i>497</i>	<i>411</i>	<i>353</i>
<i>% of CAS20</i>	<i>15.9</i>	<i>12.5</i>	<i>10.3</i>	<i>8.8</i>

The D-T CAS50 estimate of 10% of total capital is consistent with the Woodruff MIF example at 10% [4]; the p-¹¹B estimate of 6% reflects reduced spare parts, negligible fuel cost, and lighter decommissioning.

5.11 CAS60: Interest During Construction

Interest during construction (IDC) is the cost of financing the plant over the construction period. The uniform-spending IDC formula is derived in section 3.2 (eq. (5)) and applied directly here as $\text{IDC} = f_{\text{IDC}}(i, T_c) C$; at reference conditions ($i = 0.07$, $T_c = 6$ yr), $f_{\text{IDC}} = 0.192$.

To avoid double-counting construction-period financing, CAS60 and CAS90 use complementary conventions: IDC is charged explicitly in CAS60, and CAS90 applies a plain capital recovery factor to the IDC-inclusive capital,

$$\text{Total capital} = C + \text{IDC}, \quad \text{CAS90} = \text{CRF} \times \text{Total capital}. \quad (73)$$

Charging IDC as a separate line item, rather than folding it into an effective CRF, keeps it visible, uses the realistic uniform-spending assumption, and follows EMWG/ARIES cost-reporting conventions [3].

5.12 CAS70: Annualized O&M and Replacement

CAS70 comprises two sub-accounts: CAS71, annual operations and maintenance, scaled from a fuel-dependent base cost per MW of net electric capacity; and CAS72, annualized scheduled component replacement, detailed below.

5.12.1 CAS71: Staffing-Based O&M

CAS71 is set by a fuel-dependent base annual O&M cost, $C_{O\&M}(f)$ (M\$/yr at the 1 GWe reference), which is then scaled by plant size (eq. (74)). This base cost is derived from a bottom-up staffing model that estimates headcount and compensation by division (operations, maintenance, administration, technical, offsite) for each fuel type, then adds non-labor costs (maintenance materials, insurance, supplies, regulatory fees, waste treatment, and general overhead). The staffing model is grounded in two reference datasets: the S-PRISM sodium fast reactor staffing estimate [54] (494 staff for a 1,520 MWe fission plant) and INL’s first-principles SFR cost estimation [50], which scales the S-PRISM baseline to different plant sizes. Conventional gas CCGT staffing data (25–35 staff for 1 GWe) anchors the lower bound.

The key differentiator between fuels is neutron-related operational overhead. Under the Part 30 basis (section 5.1), the plant is staffed as an industrial facility with a radiation-protection and health-physics program scaled to its neutron output: fuels with higher neutron production require larger radiation-protection programs, radwaste management, and radiation-controlled maintenance, with cost scaling roughly with neutron flux. The resulting fuel-dependent coefficients are listed in table 18.

Table 18: CAS71 staffing-based O&M coefficients by fuel cycle (1 GWe reference).

Fuel	Staff	O&M (M\$/yr)	Key drivers
D-T	117	54.9	Tritium systems, HP dept, radwaste, remote handling
D-D	94	40.9	Reduced neutron flux ($\frac{1}{3}$ D-T), smaller T inventory
D- ³ He	69	27.5	5% neutron fraction, minimal tritium
p- ¹¹ B	59	24.9	Aneutronic, no tritium, RSO only

All values are at a 1 GWe reference. For comparison, S-PRISM fission O&M is \$50k/MW/yr and modern gas CCGT is \$12k/MW/yr. The pB11 estimate (\$25k/MW/yr) is approximately twice the conventional CCGT level, reflecting fusion-specific system complexity (vacuum, magnets, plasma-facing components) rather than regulatory burden.

Annual O&M scales with plant size via a power law:

$$C_{71, \text{annual}} = C_{O\&M}(f) \cdot \left(\frac{P_{\text{net}} n_{\text{mod}}}{P_{\text{ref}}} \right)^{0.5} \quad (74)$$

where the exponent 0.5 captures staffing economy of scale. The INL SFR data [50] shows staff scaling from 236 at 165 MWe to 1,040 at 3,108 MWe ($\alpha \approx 0.5$), driven by the large fixed component in administration, technical, and offsite divisions. The same exponent is used for CAS40 (section 5.9), which shares the same staffing basis. No concept-dependent factor is applied: health physics, tritium accountability, engineering, and security staffing dominate the headcount and are fuel-driven rather than geometry-driven, and no concept has a sourced maintenance-ergonomics basis to claim a discount.

5.12.2 CAS72: Scheduled Component Replacement

CAS72 covers the components that wear out during operation and must be replaced on their own schedules rather than lasting the plant life: the neutron-damaged core (first wall and blanket) for the steady-state magnetic concepts, and the driver consumables (capacitor banks, formation electrodes) for the pulsed concepts. Each replacement is charged at its cost discounted to present value at the time of the event and annualized via the CRF. For the steady-state magnetic-confinement concepts (tokamak, stellarator, mirror, steady-state FRC) the core first-wall and blanket are replaced on a neutron-fluence schedule: the core full-power-year lifetime L_{core} is the per-fuel fluence limit divided by the neutron wall loading, bounded to the plant life,

$$L_{\text{core}} = \min \left(\max \left(\frac{\Phi_{\text{max}}(f)}{q_{\text{wall}}}, L_{\text{floor}} \right), L_{\text{plant}} \right), \quad (75)$$

with Φ_{max} the fuel-dependent fluence limit (D-T 18, D-D 36, D-³He 108, p-¹¹B 180 MW yr/m²; D-T anchored to the ARIES FS 200 dpa RAFM-steel window, the others scaled by spectrum hardness), q_{wall} the neutron wall loading (neutron power per unit first-wall area), $L_{\text{floor}} = 0.5$ FPY a numerical floor, and L_{plant} the plant full-power life. A machine with higher q_{wall} exhausts its core lifetime sooner and carries a larger annualized replacement charge. The floor keeps the $1/q_{\text{wall}}$ gradient finite at extreme wall loading; the plant-life cap reflects that nothing is replaced beyond it. Limits and sources are documented in appendix E.

The set of components treated as periodically replaced is configured through the `replaceable_accounts` list (default: first wall and blanket, C220101, plus divertor, C220108). The per-event cost is the sum of those accounts’ capital,

charged every core lifetime; adding an account code to the list (for example C220103 for a thin-shield design whose coils need periodic replacement) makes that component replaceable on the same schedule:

```
from costingfe import CostModel, ConfinementConcept, Fuel
from costingfe.defaults import load_costing_constants

# add the coils (C220103) to the replaced set
cc = load_costing_constants().replace(
    replaceable_accounts=("C220101", "C220108", "C220103"),
)
model = CostModel(ConfinementConcept.TOKAMAK, Fuel.DT,
    costing_constants=cc)
```

Each replaceable item is charged as the present value of its discrete replacement series, annualized by the CRF. An item costing C_{evt} per replacement, replaced every t_{rep} years over a plant life of n years, contributes an annual charge

$$a_{\text{rep}} = \text{CRF}(i, n) C_{\text{evt}} \frac{s(1 - s^{n_{\text{rep}}})}{1 - s}, \quad s = (1 + i)^{-t_{\text{rep}}}, \quad n_{\text{rep}} = \max(0, \lceil n/t_{\text{rep}} \rceil - 1), \quad (76)$$

where $\text{CRF}(i, n)$ is the capital recovery factor (eq. (3)) and the first set is capital (already in CAS22), so only the n_{rep} later replacements are charged. CAS72 sums a_{rep} over the replaced items: the core, with $C_{\text{evt}} = n_{\text{mod}} \sum_{k \in \text{repl}} C_k$ and $t_{\text{rep}} = L_{\text{core}}/f_{\text{avail}}$ (calendar years); the DEC grid; and, for pulsed concepts, the capacitor bank and laser subsystems on their shot-derived lifetimes, plus the electrode-wear term below.

Pulsed concepts add driver-specific consumables. Inductive-DEC capacitor banks are replaced on a cycle-count and repetition-rate schedule. The electromagnetic-gun concepts (sheared-flow Z-pinch and plasma jet) replace formation electrodes, whose plasma-facing surfaces erode under high current density; because their shot lifetime can be sub-annual, the charge is levelized as an annual recurring cost rather than discrete events,

$$C_{72, \text{elec}} = c_{\text{rep}} C_{220104} \frac{N_{\text{shots/yr}}}{N_{\text{life}}}, \quad (77)$$

with $c_{\text{rep}} = 0.5$ the consumable-electrode share of the driver capital (range 0.25–0.75), $N_{\text{life}} = 10^8$ shots the electrode lifetime (range 10^7 – 10^9 , high uncertainty with no NOAK data), and $N_{\text{shots/yr}} = f_{\text{rep}} \cdot 8760 \cdot 3600 \cdot f_{\text{avail}}$ the annual shot count at repetition rate f_{rep} and availability f_{avail} ; it scales with the module count n_{mod} .

The two sub-accounts are summed,

$$\text{CAS70} = C_{71} + C_{72}, \quad (78)$$

where C_{71} is the levelized annual O&M (the base-year value of eq. (74), levelized over the plant life by section 5.14) and C_{72} the replacement charge developed above. Neglecting the growing annuity in C_{71} would underestimate the levelized cost by the percentage reported in section 5.14.

5.13 CAS80: Annualized Fuel Cost

CAS80 covers the annualized cost of fuel consumables: the burn-corrected fuel cost plus, for inertial and magneto-inertial concepts, the per-shot target consumable,

$$\text{CAS80} = A_{\text{fuel}}^{\text{eff}} + A_{\text{target}}, \quad (79)$$

with the two terms developed below ($A_{\text{target}} = 0$ for concepts with no manufactured target). These are base-year annual costs; like CAS70 they are then levelized over the plant life (section 5.14). The gross fuel expenditure A_{fuel} , before the incomplete-burn correction (eq. (81)), is computed from the fusion power, the energy per reaction, and the unit cost of the feedstock isotopes:

$$A_{\text{fuel}} = n_{\text{mod}} \cdot P_{\text{fus}} [\text{W}] \cdot \frac{8760 \times 3600 \cdot f_{\text{avail}} \cdot c_{\text{rxn}}}{Q_{\text{eff}} \cdot e_{\text{MeV}}} \quad (80)$$

where P_{fus} is in watts, c_{rxn} is the cost per fusion reaction (summing the unit costs of the feedstock isotopes weighted by their per-reaction masses), Q_{eff} is the effective energy per reaction in MeV (fuel-dependent; see table 3), and $e_{\text{MeV}} = 1.602 \times 10^{-13}$ J/MeV, and f_{avail} the plant availability (capacity factor, eq. (2)). The factor 8760×3600 converts one year to seconds. Fuel-specific unit costs are listed in table 19.

Table 19: Fuel isotope unit costs (CAS80, market purchase).

Isotope	\$/kg	Basis
Deuterium	2,175	STARFIRE (1980), inflation-adjusted
Li-6 (enriched)	1,000	90% enriched Li-6
He-3	2,000,000	Scarcity pricing
Protium	5	Commodity H ₂
B-11 (enriched)	10,000	FOAK estimate (B-10 tails)

A plant must inject more fuel than it burns. Only a fraction f_b of the injected fuel fuses per pass (the single-pass burn fraction of section 4.1); of the unburned $(1 - f_b)$, a fraction f_r is recovered from the exhaust and recycled, and the rest is lost and must be replaced with fresh feedstock. The gross cost of eq. (80) therefore understates the fuel bill: per fused reaction the make-up purchase exceeds the stoichiometric amount by $(1 - f_b)(1 - f_r)/f_b$, giving the burn-corrected fuel cost

$$A_{\text{fuel}}^{\text{eff}} = A_{\text{fuel}} \left[1 + \frac{1 - f_b}{f_b} (1 - f_r) \right] \quad (81)$$

The multiplier equals unity when either $f_b = 1$ (complete burn) or $f_r = 1$ (perfect fuel recovery). For inexpensive fuels (deuterium at \$2,175/kg) the correction is negligible; for expensive fuels (He-3 at \$2,000,000/kg) it is economically significant: at $f_b = 0.10$, $f_r = 0.95$ the effective fuel cost is $1.45\times$ the full-burn estimate, and at $f_b = 0.05$, $f_r = 0.90$ it rises to $2.9\times$.

Per-concept f_b values, with ranges and basis, are listed in appendix D; $f_r = 0.99$ is uniform across concepts. At the MFE-class point ($f_b = 0.05$) the multiplier is 1.19.

5.13.1 Target Consumable for Inertial and Magneto-Inertial Concepts

For inertial and magneto-inertial concepts the fuel-bearing consumable is not only the isotope but the fabricated target destroyed on every shot: the capsule and hohlraum of a laser or heavy-ion target, the beryllium liner and recyclable transmission line of a MagLIF or Z-pinch load. Following the fission convention, in which CAS80 holds the fabricated fuel *assembly* (cladding and structure included), not only the raw isotope, this hardware is added to CAS80 as a per-shot term parallel to eq. (80):

$$A_{\text{target}} = n_{\text{mod}} \cdot \dot{N}_{\text{shot}} \cdot c_{\text{target}}, \quad \dot{N}_{\text{shot}} = f_{\text{rep}} \cdot 8760 \times 3600 \cdot f_{\text{avail}}, \quad (82)$$

where c_{target} is the per-shot target cost (one target per shot per module), f_{rep} is the repetition rate, and f_{avail} is the plant availability (eq. (2)). The burn-fraction correction above does not apply to A_{target} : the target is consumed whole each shot regardless of fuel burnup.

c_{target} is a per-concept input, zero for magnetic concepts and for in-situ-formation pulsed concepts (section 5.3.7), and it carries only the *non-capital* per-shot cost (materials, factory operating labour, and post-shot radiological handling, divided by the acceptance yield), because the factory capital is funded once in C_{220108} (section 5.3.7). Built up this way from sub-cent materials (a diamond ablator shell, or a 3 g lead hohlraum) marked up by tritium-confined handling and divided by yield, c_{target} is about \$0.50–0.62 for laser and heavy-ion capsules and several dollars for the liner-plus-transmission-line loads (the transmission line being net of in-situ recycling).

A further consideration is that all post-shot debris is tritiated and neutron-activated, so it must be either recovered in a contained hot cell or conditioned and disposed as low-level waste; for the LIFE-standard lead hohlraum the recovered metal is worth less than the recovery facility, so single-use disposal is the default and is competitive with recycling.

Because the rep rate enters linearly, a high-rep laser plant at $f_{\text{rep}} = 10$ Hz consumes about 2.7×10^8 targets per year, so even a sub-dollar capsule contributes a several-percent share of LCOE; once the factory capital and these radiological premiums are costed explicitly rather than amortized into an optimistic sub-dollar number, the high-rep capsule concepts exceed their magnetic counterparts in LCOE, consistent with the inertial-fusion economics literature.

5.14 Levelized Annual Operating Cost

The levelization foreshadowed in section 3 is carried out here. A base-year operating cost M_0 (CAS70, CAS80) becomes a constant annual charge M_{annual} in two steps. First, it is inflated at the rate g to first-year-of-operation dollars,

$$A_1 = M_0 (1 + g)^{T_c}, \quad (83)$$

where T_c is the construction time, taken as the total project time T_{project} (eq. (38)) for first-of-a-kind plants so that the licensing delay is carried in the escalation. Second, the escalating stream is discounted at i over the plant life and annualized by the capital recovery factor (eq. (3)), giving the levelized charge

$$M_{\text{annual}} = A_1 \text{CRF}(i, n) \frac{1 - \left(\frac{1+g}{1+i}\right)^n}{i - g}, \quad (84)$$

the standard growing-annuity levelization (for the degenerate case $i = g$ the final factor reduces to $n/(1+i)$).

For example, at $M_0 = 100$ M\$, $i = 0.07$, $g = 0.02$, $n = 30$ yr, $T_c = 6$ yr, the levelized cost is 138.3 M\$/yr compared to 112.6 M\$/yr from the naïve single-year inflation formula, a 23% underestimate when the growing annuity is neglected.

5.15 CAS90: Annualized Financial Costs

CAS90 converts the total capital investment into an equivalent annual payment:

$$\text{CAS90} = \text{CRF}(i, n) \times \text{Total capital} \quad (85)$$

where total capital includes IDC (CAS60). This uses the plain CRF (eq. (3)), not the “effective CRF” $\text{CRF} \times (1+i)^{T_c}$ found in some references [2]. As discussed in section 5.11, the effective CRF is a valid convention only when CAS60 is zero; combining it with an explicit CAS60 double-counts construction financing.

In a constant-dollar framework, CAS91 (operating-period escalation) is zero by convention, and CAS92 (annual regulatory fees) is not modeled. The framework thus equates CAS90 with CAS93 (cost of money).

6 Benchmarking and Cross-Validation

`1costingfe` is exercised against two published reference designs, ARC [33] and ARIES-AT [55], as a calibration cross-check. The framework’s contribution is procurement-grounded re-derivation of the cost accounts most sensitive to fuel cycle and confinement family; divergence from heritage-scaling estimates is therefore expected, and the check is whether the divergences arise in the accounts predicted by the methodological change. All published costs are escalated to 2025 USD via the BLS Consumer Price Index (CPI-U), matching the convention used by pyFECONS [4]: a factor of 2.295 for ARIES-AT (1992 USD basis) and 1.360 for ARC (FY2014 USD basis). The operating and financial assumptions that most influence the LCOE (availability, WACC, construction time, and operating lifetime) are listed with each design’s parameters in tables 20 and 21. Both designs are run at FOAK, matching the FOAK basis of their published estimates.

6.1 ARC: Top-Level Comparison

ARC [33] is a 270 MWe demountable-coil high-field tokamak with REBCO HTS magnets and a FLiBe blanket. The inputs used are summarized in table 20. Inputs ARC does not publish (the radial-build thicknesses and power-balance auxiliaries) take the tokamak defaults.

The published fabricated-component cost is \$5,560M (FY2014 USD, [33] p. 25), or \$7,562M escalated to 2025 USD. Run at FOAK, with ARC’s REBCO coils priced at the current market (200 \$/kA-m, not the framework’s aggressive default of 50 \$/kA-m), `1costingfe` predicts a \$5,392M capital cost (19,969 \$/kWe) and a 245.2 \$/MWh LCOE, a −29 % delta.

The residual gap is the structural steel. Sorbom applies a single \$1.06M/tonne fabricated multiplier averaged across four heritage burning-plasma designs (FIRE, BPX, PCAST5, ARIES-RS), dominated by a 4,350-tonne SS316LN structural support priced at \$4.6 B (FY2014 USD, \$6.3 B escalated) — a single line that by itself exceeds `1costingfe`’s entire \$5.4 B estimate, even with the coils at the current REBCO price (\$1.58B, 29 % of capital). `1costingfe` instead builds CAS21 and CAS22 bottom-up from current procurement data, so the divergence is that heritage steel multiplier rather than the reactor equipment. The two estimates price the same steel on different bases. That multiplier is \$1,060/kg, a fabricated-fusion-component figure carried over from one-off research machines that bundles design, instrumentation, and assembly, whereas `1costingfe` prices the support as welded structural steel at commodity material (\$6/kg) plus a fabrication markup, about \$18/kg. That factor of roughly 55 (about 75 after escalating Sorbom to 2025) is a heritage-versus-commodity pricing choice for bulk steel, not a model error on either side.

Table 20: ARC inputs to `1costingfe`. Design parameters from Sorbom et al. [33]; [†] marks framework defaults ARC does not publish.

Parameter	Value	Notes
R_0	3.3 m	major radius
a	1.13 m	minor radius
κ	1.84	elongation
B_0	9.2 T	on-axis field
P_{fus}	525 MW	fusion power
P_{net}	270 MWe	net electric
Blanket	FLiBe (molten salt)	immersion; drives volume-based CAS27
Fuel	D-T	
Coils	REBCO HTS, demountable	
η_{th}	0.40 [†]	thermal conversion
REBCO conductor	200 \$/kA-m [†]	current market (\$150–300); NOAK floor 50
Availability	0.85 [†]	capacity factor
WACC i	0.07 [†]	
T_c	6 yr [†]	construction time
n	30 yr [†]	operating lifetime

6.2 ARIES-AT: Per-Account Cross-Walk

ARIES-AT [55] is a 1 GWe advanced-tokamak plant with low-temperature superconducting Nb₃Sn coils, a SiC-composite He-cooled Brayton power cycle, and a published per-account cost table that this section uses as the published-side reference. The inputs used are summarized in table 21; inputs the paper does not specify take the tokamak defaults.

Table 21: ARIES-AT inputs to `1costingfe`. Design parameters from Najmabadi and The ARIES Team [55]; [†] marks framework defaults the paper does not publish.

Parameter	Value	Notes
R_0	5.2 m	aspect ratio 4.0
a	1.3 m	
κ	2.2	
B_0	5.86 T	on-axis
P_{fus}	1755 MW	
P_{net}	1000 MWe	
η_{th}	0.59	SiC composite, Brayton
Fuel	D-T	
Coils	LTS Nb ₃ Sn	
Availability	0.85 [†]	capacity factor
WACC i	0.07 [†]	
T_c	6 yr [†]	construction time
n	30 yr [†]	operating lifetime

Table 22 compares published top-level costs (escalated to 2025 USD) with `1costingfe`’s prediction. Najmabadi and The ARIES Team [55] publishes only EMWG-style rollups (accounts 90 “Direct”, 94 “Owner’s”, 99 “Total”), not a per-account decomposition, so the cross-walk is at top-level granularity. Published direct cost maps to CAS21–27; the `1costingfe` “Overnight” row sums CAS10–50 (everything before interest during construction), and the “Total” row adds CAS60 (IDC).

Run at FOAK to match the ARIES program’s convention, `1costingfe` reproduces the published capital closely: direct cost within 1 % (+0.5 %), overnight specific cost within 6 % (−6.2 %), and total cost within 4 % (−4.0 %). The residual LCOE divergence (−23 %) is not a capital-cost difference but reflects the differing financial and O&M assumptions of the 2002 ARIES systems study (fixed-charge rate, lifetime, staffing) versus the framework defaults. Unlike ARC, ARIES-AT needs no conductor-price adjustment: its LTS Nb₃Sn coils are already priced at the mature ITER cost

Table 22: ARIES-AT cross-walk against published top-level rollups. Published costs from Najmabadi and The ARIES Team [55] Table on p. 17, escalated from 1992 USD to 2025 USD by a factor of 2.295.

Account	Published (2025 USD)	1costingfe	Δ (%)
Direct cost (Account 90), M\$	3,491	3,507	+0.5
Overnight specific cost, \$/kWe	5,602	5,257	−6.2
Total cost (Account 99), M\$	6,527	6,267	−4.0
LCOE, \$/MWh	109.1	83.6	−23.4

(7 \$/kA-m), not an aggressive NOAK target, so there is no NOAK-versus-current gap to swap as there is for ARC’s REBCO.

6.3 LCOE Composition

Figure 4 shows capital cost in M\$ broken out by major CAS account group for both reference designs side by side, computed at FOAK.

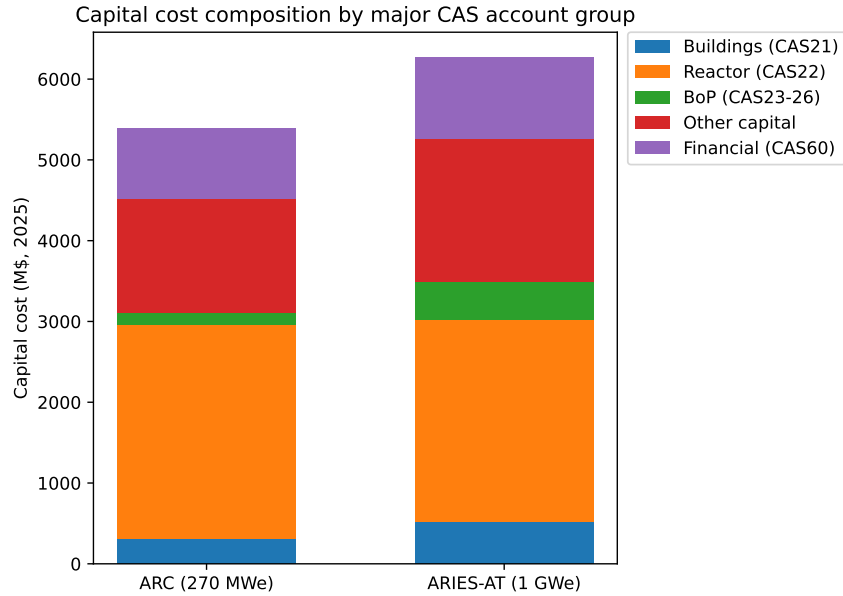


Figure 4: Capital cost composition by major CAS account group for ARC and ARIES-AT, computed by 1costingfe at FOAK. Annualised costs (CAS70 O&M, CAS80 fuel, CAS90 financial) are not included in this view; see table 22 for the full LCOE breakdown. All values in 2025 USD.

Both designs produce similar capital stacks, dominated by CAS22 (reactor plant equipment), then the aggregated indirect and owner’s costs (the “Other capital” group, including CAS30) and the CAS60 financial charge; CAS21 (buildings) is the largest direct account after the reactor. The principal difference is scale: ARC’s compact 270 MWe footprint gives a smaller absolute stack than the 1 GWe ARIES-AT but a higher \$/kWe, reflecting CAS21 and CAS30 diseconomies that do not shrink linearly with plant size.

7 Conclusion

A parsimonious differentiable framework for estimating the levelized cost of electricity from fusion power plants has been described. The framework spans the four candidate fuel cycles and the principal confinement families through a common power-balance and cost-account backbone, with each account justified independently from procurement and benchmark data rather than from heritage scaling factors alone. The differentiable backend exposes exact gradients and supports vectorised sensitivity sweeps, making LCOE-driven design exploration tractable.

Several limitations remain. The framework costs a physics operating point supplied by the user and does not bundle concept-specific 0D physics models in this release; coupling to external physics codes, or future bundled physics layers for tokamaks, stellarators, mirrors, FRCs, and inertial systems, is left to future work. Calibration cross-checks against the ARC and ARIES-AT reference designs are presented in section 6; cross-validation against pyFECONS reference cases at the per-account level is left to future work.

Acknowledgments

This work was performed within the 1cFE program at the Astera Institute Residency. The 1cFE program seeks to identify plausible corridors to fusion electricity at $\leq \$0.01/\text{kWh}$ (2025 USD); see <https://1cf.energy/>. 1costingfe is the cost-accounting layer of the program’s broader techno-economic analysis stack, developed alongside the fusion-tea repository family.

8 Code Availability

The 1costingfe source code, example scripts, and per-account documentation are released at <https://github.com/1cfe/1costingfe>. The 1cFE program landing page is available at <https://1cf.energy/>. The framework targets Python 3.11 or later and depends on JAX. Reproduction of most figures and account-level cost tables in this paper requires only the example scripts shipped in the `examples/` directory; the benchmarking results in section 6 are recorded by the scripts `benchmark_arc.py`, `benchmark_aries_at.py`, and `make_benchmarkBars.py`, located in `docs/papers/1costingfe_paper/scripts/`. The section 2 walkthrough is recorded by `examples/external_physics_handoff.py` (the rollup table) and `docs/papers/1costingfe_paper/scripts/make_tornado.py` (the sensitivity tornado figure).

A CAS10 Pre-Construction Line Items

The fixed pre-construction line items in the CAS10 build-up (eq. (36)) are flat charges, independent of plant power and module count. Table 23 lists the adopted values; the land cost (CAS11) and licensing cost (CAS13) are given in sections 5.1.1 and 5.1.2.

Table 23: Fixed CAS10 pre-construction line items.

Item	Symbol	Value (M\$)
Site permits	c_{site}	3.0
Engineering studies	c_{studies}	20.0 (FOAK), 4.0 (NOAK)
Plant permits	c_{permit}	2.0
Pre-construction reports	c_{reports}	1.0
Other	c_{other}	1.0

B Synchrotron radiation model details

This appendix documents the implementation details of the synchrotron radiation model summarized in equation (16).

B.1 Profile Assumptions and Central-Value Conversion

The Albajar model describes synchrotron radiation from a tokamak plasma and requires central (on-axis) values of electron temperature and density, whereas 1costingfe’s power balance operates on volume-averaged quantities. The assumed radial profiles follow the convention of Albajar et al. [18]:

$$T_e(\rho) = T_{e0} (1 - \rho^{\beta_T})^{\alpha_T}, \quad n_e(\rho) = n_{e0} (1 - \rho^2)^{\alpha_n} \quad (86)$$

where $\rho = r/a$ is the normalized minor radius. For profiles depending only on ρ , the toroidal volume average reduces exactly to $\langle f \rangle = 2 \int_0^1 f(\rho) \rho d\rho$ (the $(R + a\rho \cos \theta)$ Jacobian factor integrates out). For $\beta_T = 2$ (the default) this gives

$$\langle T_e \rangle = \frac{T_{e0}}{1 + \alpha_T}, \quad \langle n_e \rangle = \frac{n_{e0}}{1 + \alpha_n} \quad (87)$$

The code inverts these relations to obtain central values from the volume-averaged inputs: $T_{e0} = \langle T_e \rangle (1 + \alpha_T)$ and $n_{e0} = \langle n_e \rangle (1 + \alpha_n)$. The temperature profile shape exponent is fixed at $\beta_T = 2$ (standard parabolic profile). Default peaking exponents are $\alpha_T = 1.0$ and $\alpha_n = 0.5$, giving peaking factors of 2.0 and 1.5, respectively.

B.2 Profile Shape Factor

The profile shape factor K in equation (16) is [18], evaluated at $\beta_T = 2$:

$$K(\alpha_n, \alpha_T) = (\alpha_n + 3.87 \alpha_T + 1.46)^{-0.79} (1.98 + \alpha_T)^{1.36} 2^{2.14} (2^{1.53} + 1.87 \alpha_T - 0.16)^{-1.33} \quad (88)$$

B.3 Aspect Ratio Correction

The geometric correction factor G accounts for the finite aspect ratio of the torus [18]:

$$G(A) = 0.93 [1 + 0.85 e^{-0.82 A}] \quad (89)$$

where $A = R/a$ is the aspect ratio. In the large aspect-ratio limit $G \rightarrow 0.93$.

B.4 Application to Non-Tokamak Geometries

For stellarators the formula is applied directly using the stellarator's major and minor radii. For magnetic mirrors, which have a cylindrical geometry of length L and plasma radius a , an effective major radius is defined as

$$R_{\text{eff}} = \frac{L}{2\pi} \quad (90)$$

This maps the cylinder to a torus of equivalent volume ($V = 2\pi^2 R a^2 \kappa \rightarrow \pi a^2 L$ for $\kappa = 1$). The wall reflectivity R_w is reduced for mirrors (default 0.4 vs. 0.6 for tokamaks) to account for radiation escaping through the open ends.

C Inverse Power Balance

The costing model operates in “inverse” mode: given a target net electric output P_{net}^* , determine the required fusion power P_{fus} .

C.1 Pulsed Inverse

For pulsed concepts, Q_{eng} determines the gross electric and recirculating powers directly:

$$P_{\text{et}} = P_{\text{net}}^* \cdot \frac{Q_{\text{eng}}}{Q_{\text{eng}} - 1}, \quad (91)$$

$$P_{\text{recirc}} = P_{\text{et}} / Q_{\text{eng}}. \quad (92)$$

The driver power follows from the recirculating budget. For thermal conversion, $P_{\text{recirc}} = P_{\text{drv}} / \eta_{\text{pin}} + P_{\text{fixed}}$; for inductive DEC, $P_{\text{recirc}} = P_{\text{drv}} (1 / \eta_{\text{pin}} - 1) + P_{\text{fixed}}$, where P_{fixed} collects pumping, subsystem, auxiliary, cryogenic, target, and coil loads. Then $E_{\text{drv}} = P_{\text{drv}} / f_{\text{rep}}$, and P_{fus} is obtained from the forward energy balance with the derived E_{drv} . The inversion is closed-form (linear in P_{drv} and P_{fus}).

C.2 Steady-State Inverse

Substituting the forward power balance into eq. (28) gives $P_{\text{net}}(P_{\text{fus}})$; the inverse problem is to find the root $P_{\text{net}}(P_{\text{fus}}) = P_{\text{net}}^*$.

For fixed plasma parameters (n_e, T_e, B), the radiated power P_{rad} is independent of P_{fus} . However, the effective heating power (eq. (22)) introduces a nonlinearity: when $P_{\text{rad}} > P_{\text{cp}} + P_{\text{in}}$, the effective heating depends on $P_{\text{cp}} = f_{\text{cp}} P_{\text{fus}}$ (where f_{cp} is the charged-particle fraction), making $P_{\text{in,eff}}$ a function of P_{fus} . The net electric power is therefore piecewise linear in P_{fus} , with two regimes:

1. **Uncapped** ($P_{\text{rad}} < P_{\text{cp}} + P_{\text{in}}$): $P_{\text{in,eff}} = P_{\text{in}}$ (constant); the forward balance is linear in P_{fus} and admits a closed-form solution.
2. **Radiation-limited** ($P_{\text{rad}} \geq P_{\text{cp}} + P_{\text{in}}$): $P_{\text{in,eff}} = P_{\text{rad}} - f_{\text{cp}} P_{\text{fus}}$; the forward balance is linear with a different slope (increasing P_{fus} provides more ash power to offset radiation, reducing required heating).

The inverse solver uses Newton iteration with an analytical piecewise-constant Jacobian, initialized from the closed-form uncapped solution. Because $P_{\text{net}}(P_{\text{fus}})$ is piecewise linear, convergence is exact in at most two iterations. The Newton step is:

$$P_{\text{fus}}^{(k+1)} = P_{\text{fus}}^{(k)} - \frac{P_{\text{net}}(P_{\text{fus}}^{(k)}) - P_{\text{net}}^*}{\left. \frac{dP_{\text{net}}}{dP_{\text{fus}}} \right|_{P_{\text{fus}}^{(k)}}} \quad (93)$$

where the derivative is computed analytically for each regime rather than via automatic differentiation, avoiding nested differentiation during sensitivity analysis.

D Per-Concept Burn Fraction and Fuel Recovery

This appendix collects the per-concept single-pass burn fraction f_b (burn_fraction) introduced in section 4.1, with a plausible design range and basis for each. Values are reactor-target (NOAK) design points, not experimental records: f_b is bounded above by kinematic and confinement physics and fixed by operating-point design. Several entries are design-regime estimates with concept-specific sourcing still pending, and the electrostatic concepts (orbitron, polywell) carry MFE-class placeholders in the absence of a public reactor-scale study.

Table 24: Single-pass burn fraction f_b by concept, with plausible design range and basis (reactor-target NOAK values).

Concept	f_b	Range	Basis
Tokamak, stellarator, mirror	0.05	0.02–0.10	Shared moderate- $n\tau$ single-pass MFE regime; tokamak and stellarator reactor studies [55, 34], mirror a modern axisymmetric tandem [56] (legacy MFTF/TARA quote 1–3%).
Orbitron, polywell	0.05	n/a	MFE-class placeholder; no public reactor-scale study.
Laser IFE	0.25	0.10–0.35	Laser-ICF reactor studies (LIFE, HAPL) [57, 58].
Heavy-ion IFE	0.30	0.20–0.40	Indirect-drive heavy-ion fusion (HIBALL) [59]; higher uniformity than direct drive.
Pulsed FRC	0.15	0.10–0.25	Magneto-inertial regime midpoint; Helion-class staged-compression FRC reports gain Q , not f_b [60].
MagLIF	0.15	0.08–0.25	2D radiation-MHD projections at full Z-driver [61].
Magnetized target	0.10	0.05–0.15	Acoustically-driven magnetized-target reactor projections [62].
Plasma jet (PJMIF)	0.10	0.05–0.15	Plasma-jet-driven MIF simulations [63].
Staged Z-pinch	0.10	0.05–0.15	LANL staged-pinch designs; sourcing pending.
Z-pinch (IFE)	0.10	0.05–0.15	Rayleigh–Taylor disassembly limit.
Theta pinch	0.05	0.03–0.08	Faster expansion than Z-pinch; closer to the MFE bound.
Dense plasma focus	0.01	0.005–0.02	Sub-microsecond pinch lifetime is binding [25]; the value is low and materially raises DPF LCOE.

Unburned fuel is recovered and recycled with efficiency f_r (fuel_recovery), taken as a uniform NOAK value of 0.99 across all concepts. ITER targets 99% tritium recovery as the mature reference; the within-concept architectural spread (gas-phase exhaust versus target-factory residue) is at most about five percentage points at NOAK; and sensitivity to f_r is highest at low f_b , exactly where concepts are most architecturally similar (all gas-phase MFE). A FOAK/NOAK-toggled f_r (e.g. 0.95/0.99) is a future refinement.

E First-Wall Fluence Limits

The fuel-dependent neutron fluence limits Φ_{max} of eq. (75) set the fluence-based core-replacement lifetime for the steady-state magnetic concepts. This appendix records their basis. No value here is taken from or calibrated against a cost-modeling tool; all numbers come from peer-reviewed papers and fusion power-plant design studies.

The end-of-life limit for a reduced-activation ferritic/martensitic (RAFM) steel first wall and blanket is set by displacement damage in the structural steel, with a widely used design limit of 200 dpa, beyond which embrittlement and loss of fracture toughness make the structure unacceptable. The ARIES nuclear assessment ties this to a fluence: the ferritic-steel structure ends its service life at 200 dpa, corresponding to 18 MW yr/m² of first-wall neutron fluence [64, 65], about 11 dpa per MW yr/m². Independent cross-checks constrain this window: the ARIES-AT SiC/SiC option reaches 18.5 MW yr/m² at its 3% burnup limit [64], and the EU-DEMO starter blanket is specified for 2 MW yr/m² at about 20 dpa (10 dpa per MW yr/m²) [66], placing the RAFM end-of-life window at 15–20 MW yr/m². The D-T reference adopts 18 MW yr/m².

The per-fuel values scale with spectrum hardness [67]: a softer neutron spectrum does less displacement damage per unit fluence, reaching the 200 dpa limit at higher fluence.

Table 25: Per-fuel first-wall neutron fluence limit Φ_{\max} and basis.

Fuel	Φ_{\max} [MW yr/m ²]	Basis
D-T	18	ARIES ferritic-steel 200 dpa = 18 MW yr/m ² [64, 65]; cross-checked by ARIES-AT SiC and EU-DEMO. Primary source.
D-D	36	2× D-T: 2.45 MeV neutrons do roughly half the dpa per unit fluence of 14.1 MeV neutrons [67]. Direction sourced; the factor of 2 is a modeling choice.
D- ³ He	108	6× D-T: neutron load is only the few-percent D-D side channel, so the steel is effectively never fluence-limited. Magnitude a placeholder; the ordering is physical.
p- ¹¹ B	180	10× D-T: aneutronic to within a small side yield. Placeholder magnitude; the ordering is physical.

Only the D-T value is anchored to a primary structural-limit source. The D-D factor follows the sourced spectrum direction, but its magnitude is a modeling choice; the D-³He and p-¹¹B values are deliberately large placeholders encoding “not fluence-limited” (for these fuels the plant-life clamp binds first). EUROFER97 has been characterized to about 80 dpa [68] while the 200 dpa limit is a design extrapolation, the largest single materials uncertainty behind the basis. The damage limits are sourced from tokamak and generic-blanket studies; the material limits carry over to other geometries, but the plasma-to-wall mapping is specific to the present model.

F Reference Walkthrough Script

The full reference script for the section 2 walkthrough is reproduced below. It is the canonical 1 GWe D-³He steady-state mirror reference cited in tables 1 and 2, and lives in the repository at `examples/external_physics_handoff.py`.

```
"""Canonical 1 GWe D-3He steady-state mirror reference for the 1costingfe paper.
```

```
This is the example cited in Section 2.2: physics outputs from an external
model (central-cell geometry, field, temperatures, densities, DEC fractions,
secondary burn fractions) hand off to the 1costingfe forward call, which
produces a complete CAS-account rollup and an LCOE figure.
```

```
The forward call uses an inverse power-balance solve: given the engineering
parameters (geometry, efficiencies, burn fractions) and the net electric
target, the model finds the required fusion power and derives all costs.
```

```
Numbers are illustrative; the point is the handoff pattern, not the design.
"""
```

```
from costingfe import ConfinementConcept, CostModel, Fuel, PowerCycle
```

```
def main() -> None:
    model = CostModel(
        concept=ConfinementConcept.MIRROR,
        fuel=Fuel.DHE3,
        power_cycle=PowerCycle.RANKINE,
```

```

)

result = model.forward(
    # Customer parameters
    net_electric_mw=1000.0,
    availability=0.85, # default plant availability (ARIES heritage)
    lifetime_yr=30,
    construction_time_yr=6.0,
    interest_rate=0.07,
    inflation_rate=0.02,
    noak=True,
    # Geometry (Section 2.2 Table: central-cell length, plasma radius)
    R0=0.0, # cylinder axis (no major-radius offset)
    chamber_length=80.0, # m, central-cell length
    plasma_t=0.4, # m, plasma radius at midplane
    elon=1.0, # circular cross-section
    blanket_t=0.30, # m, thin blanket (D-3He: low neutron fluence)
    ht_shield_t=0.20, # m
    structure_t=0.15, # m
    vessel_t=0.10, # m
    # Magnets
    b_center=12.0, # T, on-axis field at the coil center
    r_bore=1.85, # m, effective winding bore radius
    # Power balance (Section 2.2 Table)
    p_input=50.0, # MW, NBI heating (neutral beams sustain mirror)
    eta_couple=1.0, # NBI coupling; eta_pin = 0.60 x 1.0 = 0.60
    eta_p=0.50, # pumping efficiency
    p_coils=5.0, # MW, solenoid + mirror coils
    p_cool=25.0, # MW, first-wall cooling
    p_pump=1.5, # MW
    p_house=4.0, # MW
    p_cryo=1.0, # MW
    f_sub=0.03, # BOP subsystem fraction
    # Blanket / neutronics: D-3He is aneutronic primary, no blanket needed
    blanket_form="none",
    blanket_fill="none",
    mn=1.0, # no neutron multiplication without a breeding blanket
    # Conversion: venetian-blind DEC on end-loss ions + thermal
    # (eta_th supplied by the RANKINE preset on CostModel)
    eta_de=0.70, # venetian-blind DEC efficiency on end-loss ions
    f_dec=0.90, # fraction of transport power routed to DEC
    # Plasma parameters for radiation calculation (Section 2.2 Table)
    n_e=3.3e19, # m^-3, electron density
    T_e=70.0, # keV, electron temperature
    Z_eff=1.3, # effective ion charge
    B=3.0, # T, central-cell field
    plasma_volume=400.0, # m^3 (pi * plasma_t^2 * chamber_length)
    T_edge=0.20, # keV, edge temperature (open field lines)
    tau_ratio=3.0, # impurity confinement time / energy confinement time
    R_w=0.4, # wall reflectivity (lower for open ends)
    # D-3He secondary burn fractions (Section 2.2 Table)
    dhe3_f_T=0.5, # secondary D-T burn fraction
    dhe3_dd_frac=0.131, # D-D side-reaction fraction
    dd_f_T=0.969,
    dd_f_He3=0.689,
)

costs = result.costs
pt = result.power_table

# Group-level rollup (matches paper Section 2.2 table)
# CAS20 = sum of CAS21-29 (direct capital); CAS30 is indirect, shown separately.
cas23_29 = (
    costs.cas23
    + costs.cas24

```



```

    + costs.cas25
    + costs.cas26
    + costs.cas27
    + costs.cas28
    + costs.cas29
)
rows = [
    ("CAS10", costs.cas10),
    ("CAS21", costs.cas21),
    ("CAS22", costs.cas22),
    ("CAS23-29", costs.cas23_29),
    ("CAS30", costs.cas30),
    ("CAS40", costs.cas40),
    ("CAS50", costs.cas50),
    ("CAS60", costs.cas60),
    ("Total overnight", costs.total_capital),
    ("CAS70 (M$/yr)", costs.cas70),
    ("CAS80 (M$/yr)", costs.cas80),
    ("CAS90 (M$/yr)", costs.cas90),
    ("LCOE", costs.lcoe),
]
print("1 GWe D-3He mirror with venetian-blind DEC, NOAK reference\n")
for label, value in rows:
    print(f" {label:<25s} {float(value):>10.1f}")
print()
print("Power balance:")
print(f" P_fus: {pt.p_fus:.0f} MW")
print(f" P_net: {pt.p_net:.0f} MW")
print(f" Q_eng: {pt.q_eng:.2f}")
print(f" Recirc: {pt.rec_frac:.1%}")
print()
print(f"Overnight specific cost: {costs.capital_per_kw:.0f} $/kW")
print(f"LCOE: {costs.lcoe:.1f} $/MWh")

if __name__ == "__main__":
    main()

```

References

- [1] S. C. Schulte, T. L. Willke, and J. R. Young. Fusion reactor design studies — standard accounts for cost estimates. Technical Report PNL-2648, Battelle Pacific Northwest Laboratory, May 1978. URL <https://www.osti.gov/servlets/purl/6635206>. OSTI 6635206.
- [2] R. L. Miller. Economic goals and requirements for competitive fusion energy. *Fusion Engineering and Design*, 41:393–400, 1998. doi:[10.1016/S0920-3796\(98\)00120-3](https://doi.org/10.1016/S0920-3796(98)00120-3).
- [3] GEN-IV Economic Modeling Working Group. Cost estimating guidelines for generation IV nuclear energy systems. Technical Report Rev. 4.2, Generation IV International Forum, 2007. GIF/EMWG/2007/004.
- [4] Simon Woodruff. A costing framework for fusion power plants. *arXiv preprint*, January 2026. URL <https://arxiv.org/abs/2601.21724>.
- [5] Simon Woodruff, Alicia Durham, Alex Higginbottom, and Chris Raastad. Extension of the fusion power plant costing standard. *arXiv preprint*, February 2026. URL <https://arxiv.org/abs/2602.19389>.
- [6] Philip Eash-Gates, Magdalena M. Klemun, Goksin Kavlak, James McNerney, Jacopo Buongiorno, and Jessika E. Trancik. Sources of cost overrun in nuclear power plant construction call for a new approach to engineering design. *Joule*, 4(11):2348–2373, November 2020. doi:[10.1016/j.joule.2020.10.001](https://doi.org/10.1016/j.joule.2020.10.001).
- [7] S. J. Frank, C. J. Perks, A. O. Nelson, T. Qian, S. Jin, A. Cavallaro, A. Rutkowski, A. Reiman, J. P. Freidberg, P. Rodriguez-Fernandez, and D. G. Whyte. Radiative pulsed L-mode operation in ARC-class reactors. *Nuclear Fusion*, 62(12):126036, 2022. doi:[10.1088/1741-4326/ac95ac](https://doi.org/10.1088/1741-4326/ac95ac).
- [8] J. D. Huba. *NRL Plasma Formulary*. Naval Research Laboratory, 2016. NRL/PU/6790–16-614.

- [9] H.-S. Bosch and G. M. Hale. Improved formulas for fusion cross-sections and thermal reactivities. *Nuclear Fusion*, 32(4):611–631, 1992. doi:[10.1088/0029-5515/32/4/107](https://doi.org/10.1088/0029-5515/32/4/107).
- [10] V. F. Dmitriev. α -particle spectrum in the reaction $p + {}^{11}\text{B} \rightarrow \alpha + {}^8\text{Be}^* \rightarrow 3\alpha$. *Physics of Atomic Nuclei*, 72(7):1165–1167, 2009. doi:[10.1134/S1063778809070084](https://doi.org/10.1134/S1063778809070084).
- [11] R. M. Prior, M. C. Spraker, R. H. France, S. Stave, M. W. Ahmed, H. J. Karwowski, J. M. Mueller, L. S. Myers, and H. R. Weller. The total cross sections of the ${}^{11}\text{B}(\alpha, n){}^{14}\text{N}$ and the ${}^{10}\text{B}(\alpha, n){}^{13}\text{N}$ reactions between 2 and 6 MeV. *Nuclear Science and Techniques*, 28:106, 2017. doi:[10.1007/s41365-017-0265-0](https://doi.org/10.1007/s41365-017-0265-0).
- [12] S. V. Putvinski, D. D. Ryutov, and P. N. Yushmanov. Fusion reactivity of the p-B11 plasma revisited. *Nuclear Fusion*, 59(7):076018, 2019. doi:[10.1088/1741-4326/ab1a60](https://doi.org/10.1088/1741-4326/ab1a60).
- [13] I. E. Ochs, E. J. Kolmes, and N. J. Fisch. Preventing ash from poisoning proton-boron-11 fusion. *Physics of Plasmas*, 32(5):052506, 2025. doi:[10.1063/5.0266369](https://doi.org/10.1063/5.0266369).
- [14] Heinrich Hora, Shalom Eliezer, and Noaz Nissim. Elimination of secondary neutrons from laser proton-boron fusion. *Laser and Particle Beams*, 2021:e13, 2021. doi:[10.1155/2021/9978899](https://doi.org/10.1155/2021/9978899).
- [15] John Wesson. *Tokamaks*. Oxford University Press, 4th edition, 2011. ISBN 978-0-19-959223-4.
- [16] T. H. Rider. Fundamental limitations on plasma fusion systems not in thermodynamic equilibrium. *Physics of Plasmas*, 4:1039–1046, 1997. doi:[10.1063/1.872556](https://doi.org/10.1063/1.872556).
- [17] I. E. Ochs, E. J. Kolmes, M. E. Mlodik, T. Rubin, and N. J. Fisch. Improving the feasibility of economical proton-boron-11 fusion via alpha channeling with a hybrid fast and thermal proton scheme. *Physical Review E*, 106(5):055215, 2022. doi:[10.1103/PhysRevE.106.055215](https://doi.org/10.1103/PhysRevE.106.055215).
- [18] F. Albajar, J. Johnner, and G. Granata. Improved calculation of synchrotron radiation losses in realistic tokamak plasmas. *Nuclear Fusion*, 41(6):665–678, 2001. doi:[10.1088/0029-5515/41/6/301](https://doi.org/10.1088/0029-5515/41/6/301).
- [19] I. Fidone, G. Giruzzi, and G. Granata. Synchrotron radiation loss in tokamaks of arbitrary geometry. *Nuclear Fusion*, 41(12):1755–1758, 2001. doi:[10.1088/0029-5515/41/12/102](https://doi.org/10.1088/0029-5515/41/12/102).
- [20] I. E. Ochs, M. E. Mlodik, and N. J. Fisch. Electron tail suppression and effective collisionality due to synchrotron emission and absorption in mildly relativistic plasmas. *Physics of Plasmas*, 31(8):083303, 2024. doi:[10.1063/5.0228464](https://doi.org/10.1063/5.0228464).
- [21] J. Bohdansky. A universal relation for the sputtering yield of monatomic solids at normal ion incidence. *Nuclear Instruments and Methods in Physics Research Section B*, 2(1–3):587–591, 1984. doi:[10.1016/0168-583X\(84\)90271-4](https://doi.org/10.1016/0168-583X(84)90271-4).
- [22] Wolfgang Eckstein. *Sputtering by Particle Bombardment: Experiments and Computer Calculations from Threshold to MeV Energies*, volume 110 of *Topics in Applied Physics*. Springer, 2007. doi:[10.1007/978-3-540-44502-9](https://doi.org/10.1007/978-3-540-44502-9).
- [23] D. E. Post, R. V. Jensen, C. B. Tarter, W. H. Grasberger, and W. A. Lokke. Steady-state radiative cooling rates for low-density, high-temperature plasmas. *Atomic Data and Nuclear Data Tables*, 20(5):397–439, 1977. doi:[10.1016/0092-640X\(77\)90026-2](https://doi.org/10.1016/0092-640X(77)90026-2).
- [24] A. A. Mavrin. Improved fits of coronal radiative cooling rates for high-temperature plasmas. *Radiation Effects and Defects in Solids*, 173(5–6):388–398, 2018. doi:[10.1080/10420150.2018.1462361](https://doi.org/10.1080/10420150.2018.1462361).
- [25] E. J. Lerner et al. Focus fusion: overview of progress towards p-B11 fusion with the dense plasma focus. *Journal of Fusion Energy*, 2023. doi:[10.1007/s10894-023-00345-z](https://doi.org/10.1007/s10894-023-00345-z).
- [26] Virginia Department of Energy. Chesterfield ARC pilot plant site filing, 2024. 100 acres for 400 MWe planned capacity.
- [27] U.S. Nuclear Regulatory Commission. Licensing and regulating fusion energy systems (secy-23-0001 and commission affirmation), 2023. URL <https://www.nrc.gov/reading-rm/doc-collections/commission/secys/2023/2023-0001scy.pdf>. Decision to regulate near-term fusion energy systems under 10 CFR Part 30 (byproduct materials).
- [28] Cushman & Wakefield. U.S. Industrial MarketBeat. Cushman & Wakefield Research, 2025. Quarterly U.S. industrial real-estate market report; benchmark for industrial-grade construction and land cost.
- [29] National Energy Technology Laboratory. Cost and performance baseline for fossil energy plants, volume 1: Bituminous coal and natural gas to electricity. Technical Report DOE/NETL-2022/3575, U.S. Department of Energy, NETL, October 2022. URL <https://netl.doe.gov/NETLVol1BaselineTool>. Revision 4a.
- [30] National Renewable Energy Laboratory. Annual technology baseline — nuclear. Technical report, NREL, 2024. URL <https://atb.nrel.gov/electricity/2024/nuclear>.

- [31] Arnulf Grubler. The costs of the French nuclear scale-up: A case of negative learning by doing. *Energy Policy*, 38(9):5174–5188, September 2010. doi:[10.1016/j.enpol.2010.05.003](https://doi.org/10.1016/j.enpol.2010.05.003).
- [32] Jessica R. Lovering, Arthur Yip, and Ted Nordhaus. Historical construction costs of global nuclear power reactors. *Energy Policy*, 91:371–382, April 2016. doi:[10.1016/j.enpol.2016.01.011](https://doi.org/10.1016/j.enpol.2016.01.011).
- [33] B. N. Sorbom, J. Ball, T. R. Palmer, F. J. Mangiarotti, J. M. Sierchio, P. Bonoli, C. Kasten, D. A. Sutherland, H. S. Barnard, C. B. Haakonsen, J. Goh, C. Sung, and D. G. Whyte. ARC: A compact, high-field, fusion nuclear science facility and demonstration power plant with mountable magnets. *Fusion Engineering and Design*, 100:378–405, 2015. doi:[10.1016/j.fusengdes.2015.07.008](https://doi.org/10.1016/j.fusengdes.2015.07.008).
- [34] F. Najmabadi and The ARIES Team. The ARIES-CS compact stellarator fusion power plant. *Fusion Science and Technology*, 54(3):655–672, 2008. doi:[10.13182/FST54-655](https://doi.org/10.13182/FST54-655).
- [35] G. H. Neilson, C. O. Gruber, J. H. Harris, D. J. Rej, R. T. Simmons, and R. L. Strykowski. Lessons learned in risk management on NCSX. Technical Report PPPL-4455, Princeton Plasma Physics Laboratory, 2010.
- [36] T. M. Anklam, A. J. Simon, S. Powers, and W. R. Meier. LIFE: The case for early commercialization of fusion energy. *Fusion Science and Technology*, 60(1):66–71, 2011. doi:[10.13182/FST10-323](https://doi.org/10.13182/FST10-323).
- [37] ExxonMobil. Three new hydrocracker reactors arrive at ExxonMobil Rotterdam refinery. ExxonMobil Basestocks news, 2017. URL <https://www.exxonmobil.com/en/basestocks/news-insights-and-resources/exxonmobil-rotterdam-refinery-hydrocracker-reactors>. Three reactors, 4.5 m diameter, 25–30 m tall; full hydrocracker unit investment over \$1B.
- [38] Midcontinent Independent System Operator. Transmission cost estimation guide for MTEP24. Technical report, MISO, May 2024. URL <https://cdn.misoenergy.org/20240501%20PSC%20Item%2004%20MISO%20Transmission%20Cost%20Estimation%20Guide%20for%20MTEP24632680.pdf>. Table 2.4-2: VSC HVDC valve hall \$83.4M at ± 250 kV / 500 MW; \$266.4M at ± 400 kV / 1.5 GW.
- [39] Fusion for Energy. Europe delivers eight ITER cryopumps. F4E News, 2024. URL <https://fusionforenergy.europa.eu/news/europe-delivers-eight-iter-cryopumps/>. Eight torus and cryostat cryopumps; F4E investment EUR 21 M; manufactured by Research Instruments / Alsymex consortium.
- [40] R. S. Hemsworth, D. Boilson, P. Blatchford, M. Dalla Palma, G. Chitarin, H. P. L. de Esch, F. Geli, M. Dremel, J. Graceffa, D. Marcuzzi, G. Serianni, D. Shah, M. Singh, M. Urbani, and P. Zaccaria. Overview of the design of the ITER heating neutral beam injectors. *New Journal of Physics*, 19(2):025005, 2017. doi:[10.1088/1367-2630/19/2/025005](https://doi.org/10.1088/1367-2630/19/2/025005). URL <https://iopscience.iop.org/article/10.1088/1367-2630/19/2/025005>.
- [41] M. A. Hoffman. Electrostatic direct energy converter performance and cost scaling laws. Technical Report UCID-17560, Lawrence Livermore Laboratory, 1977. URL <https://www.osti.gov/biblio/7218298>.
- [42] W. L. Barr and R. W. Moir. Test results on plasma direct converters. *Fusion Technology*, 3(1):98–111, 1983. doi:[10.13182/FST83-A20820](https://doi.org/10.13182/FST83-A20820).
- [43] L. M. Waganer. ARIES cost account documentation. Technical Report UCSD-CER-13-01, University of California, San Diego, June 2013. URL <https://qedfusion.org/LIB/REPORT/ARIES-ACT/UCSD-CER-13-01.pdf>.
- [44] U.S. Department of Energy. Quadrennial technology review 2015, chapter 4r: Supercritical carbon dioxide brayton cycle. Technical report, U.S. Department of Energy, 2015. URL <https://www.energy.gov/sites/prod/files/2016/06/f32/QTR2015-4R-Supercritical-Carbon-Dioxide-Brayton%20Cycle.pdf>.
- [45] Sandia National Laboratories. Advanced energy conversion. <https://energy.sandia.gov/programs/nuclear-energy/advanced-energy-conversion/>, 2024. Accessed March 2026.
- [46] North China Electric Power University. Economic comparison between sCO₂ power cycle and water-steam Rankine cycle. Technical report, North China Electric Power University, 2021. URL <https://bjmfht.ncepu.edu.cn/docs/2021-12/19cd8e0ecf474f31a0efcfd9f1175415.pdf>.
- [47] ARPA-E. GEMINA: Generating electricity managed by intelligent nuclear assets. U.S. Department of Energy, Advanced Research Projects Agency–Energy, 2020. URL <https://arpa-e.energy.gov/technologies/programs/gemina>. Program awards: nine advanced-reactor digital-twin projects, \$27 M total; U. Michigan scalable reactor digital twin \$5.2 M.
- [48] S. J. Piet. Inherent/passive safety for fusion. *Fusion Technology*, 10(3P2B):1191–1196, November 1986. doi:[10.13182/FST86-A24892](https://doi.org/10.13182/FST86-A24892). OSTI 7005793.
- [49] B. G. Logan. A rationale for fusion economics based on inherent safety. *Journal of Fusion Energy*, 4(4):245–267, 1985. doi:[10.1007/BF01053357](https://doi.org/10.1007/BF01053357).

- [50] Jacob H. Prosser, Max Graham, Yaset Acevedo, Mark Jensen, Brian D. James, and Abdalla Abou-Jaoude. First-principles cost estimation of a sodium fast reactor nuclear plant. Technical Report INL/RPT-23-74316, Revision 1, Idaho National Laboratory, January 2024. https://inldigitallibrary.inl.gov/sites/sti/sti/Sort_67398.pdf.
- [51] World Nuclear Association. Economics of nuclear power, 2025. URL <https://world-nuclear.org/information-library/economic-aspects/economics-of-nuclear-power>. Accessed March 2026.
- [52] OECD Nuclear Energy Agency. Costs of decommissioning nuclear power plants. Technical Report NEA No. 7201, OECD/NEA, 2016. URL <https://www.oecd-neo.org/upload/docs/application/pdf/2019-12/7201-costs-decom-npp.pdf>.
- [53] International Atomic Energy Agency. Decommissioning and waste management considerations for fusion. Technical Report IAEA-TECDOC-2116, IAEA, 2020. URL <https://www-pub.iaea.org/MTCD/publications/PDF/TE-2116web.pdf>.
- [54] Charles E. Boardman, Marvin Hui, Douglas G. Carroll, and Allen E. Dubberley. Economic assessment of S-PRISM including development and generating costs. In *Proceedings of the 9th International Conference on Nuclear Engineering (ICONE-9)*, 2000. https://inis.iaea.org/collection/NCLCollectionStore/_Public/33/020/33020128.pdf.
- [55] F. Najmabadi and The ARIES Team. The ARIES-AT advanced tokamak, advanced technology fusion power plant. *Fusion Engineering and Design*, 80(1–4):3–23, 2006. doi:10.1016/j.fusengdes.2005.11.003.
- [56] S. J. Frank et al. Confinement performance predictions for a high field axisymmetric tandem mirror. *arXiv preprint*, 2024. URL <https://arxiv.org/abs/2411.06644>.
- [57] E. I. Moses et al. A sustainable nuclear fuel cycle based on laser inertial fusion energy. *Fusion Science and Technology*, 56:547–565, 2009.
- [58] J. D. Sethian et al. The science and technologies for fusion energy with lasers and direct-drive targets. *IEEE Transactions on Plasma Science*, 38(4):690–703, 2010.
- [59] B. Badger et al. HIBALL-II: An improved conceptual heavy ion beam driven reactor study. Technical Report UWFD-625, University of Wisconsin Fusion Technology Institute, 1984.
- [60] J. Slough et al. A compact fusion reactor based on staged compression of an FRC. *Nuclear Fusion*, 2024. doi:10.1088/1741-4326/ae034d.
- [61] S. A. Slutz et al. Pulsed-power-driven cylindrical liner implosions of laser preheated fuel magnetized with an axial field. *Physics of Plasmas*, 17(5):056303, 2010. doi:10.1063/1.3333505.
- [62] M. Laberge. An acoustically driven magnetized target fusion reactor. *Journal of Fusion Energy*, 26:179–182, 2007. doi:10.1007/s10894-007-9091-4.
- [63] S. C. Hsu et al. Plasma-jet-driven magneto-inertial fusion. *Fusion Science and Technology*, 2019.
- [64] L. A. El-Guebaly and The ARIES Team. Nuclear performance assessment of ARIES-AT. ARIES-AT final report, UC San Diego / Univ. Wisconsin, 2006.
- [65] L. A. El-Guebaly and The ARIES Team. Nuclear issues and analysis for ARIES. Technical Report UWFD-1108, University of Wisconsin Fusion Technology Institute, 1999.
- [66] L. V. Boccaccini et al. Objectives and status of EUROfusion DEMO blanket studies. *Fusion Engineering and Design*, 2016.
- [67] A. Yu. Konobeyev et al. Iron NRT- and arc-displacement cross sections and their covariances. *Nuclear Materials and Energy*, 2017. doi:10.1016/j.nme.2017.07.006.
- [68] E. Gaganidze et al. Assessment of neutron irradiation effects on RAFM steels. *Fusion Engineering and Design*, 2012. doi:10.1016/j.fusengdes.2012.04.052.